OSTBC MIMO Transceiver System for radio signal propagation challenges over irregular terrain in the Northern Cape, South Africa

Xolani Brightness Maxama

Submitted in fulfilment of the requirements for the degree:

Master of Engineering in Electrical Engineering

in the Department of Electrical, Electronic and Computer Engineering

Faculty of Engineering, Built Environment and Information Technology

Central University of Technology, Free State

Supervisor: Dr E. D. Markus

2020

Declaration

I, the undersigned, hereby declare that the work contained in this dissertation submitted for the degree of MASTER OF ENGINEERING IN ELECTRICAL ENGINEERING, is my own independent work, and has not been submitted before at any institution for a degree.

……

Signature of Student

X. B. Maxama

Acknowledgments

I am deeply grateful to our Heavenly Father for the help and inspiration granted me to complete this research.

Thank you to my Supervisor, Dr Elisha Didam Markus for the guidance, encouragement and knowledge in channelling my thoughts and faculties to be able to complete this research.

I would also like to express my love and appreciation for my family members who have been a great source of support and encouragement during my studies.

Finally, I would like to thank the Eskom business for affording me the opportunity and financial resources to undertake this research.

Abstract

The Northern Cape Province in South Africa, along the Orange River valley, has radio signal reception challenges due to high mountain ranges. The South African Electricity Authority- Eskom has High Voltage assets to monitor in this region. However, due to radio signal reception challenges, it is impossible to monitor their assets via the Supervisory Control and Data Acquisition (SCADA) system.

This research aims at developing a Very-High Frequency Orthogonal Space – Time Block Code Multiple-In Multiple-Out (VHF OSTBC MIMO) transceiver simulation model over a Rayleigh fading channel to address the radio communication challenges along the Orange River. The transceiver simulation model will resemble the harsh multipath environment presented by the mountainous terrain in the Northern Cape Province.

In environments with irregular terrain such as hills and mountains, the radio signal comes across phenomena such as reflection, refraction, diffraction and scattering. Therefore, the transmitted radio signal undergoes heavy fading and inter-symbol interference (ISI), thus negatively impacting radio link performance. However, the Multiple-input- multiple-output (MIMO) system, which uses multiple antennas both at the transmitter and receiver, takes advantage of this drawback and makes use of the high levels of multi-paths to operate at an optimum. MIMO creates spatial diversity which accounts for better radio link performance, it also yields increased capacity and improves Signal-to-Noise Ratio (SNR) while reducing bit errors.

Therefore, MIMO is one of the systems of interest considered best to exploit in this research. Space- time coding (STC) has also been considered because of its ability to increase the reliability of the channel and for its signal decoding simplicity at the receiver. A suitable lower frequency band to use for this research was also investigated. The most attractive characteristic of the low frequency (LF) band that was sought after was its ability to easily diffract over large obstacles than higher frequencies. The Very High Frequency (VHF) band at 70 MHz was found to meet the requirements for the model used.

Therefore, this dissertation presents the simulation results of a VHF OSTBC MIMO transceiver model over a Rayleigh fading channel that is typical of the mountainous regions of the Northern Cape Province in South Africa, to help overcome radio signal reception challenges.

The following are the different component blocks that made up the model: Random Binary Generator (RBG), Quadrature Phase Shift Key (QPSK) Modulator, Orthogonal Space-Time Block Code (OSTBC) Encoder, Multiple-In Multiple-Out (MIMO) Rayleigh Fading Channel, Added White Gaussian Noise (AWGN), Orthogonal Space-Time Block Code (OSTBC) Decoder and a Quadrature Phase Shift Key (QPSK) Demodulator.

The simulation results in this research were generated using the following software packages namely: Matlab/Simulink, Atoll Wireless Network and Pathloss 4 Network. The Matlab/Simulink software was used to determine the bit-error-rate (BER) performance of four different OSTBC MIMO systems, each using different antenna arrays. The Matlab RF Propagation Tool-SiteViewer was used to generate coverage predictions and receive signal strength (RSS) levels of three VHF OSTBC MIMO systems operating at three different low VHF frequency bands. The Atoll Wireless Network software was used to generate coverage plot predictions. The Pathloss 4 software was used to generate Line of Sight (LoS) predictions.

The results have shown that employing the low band VHF OSTBC MIMO transceiver system in irregular terrain environments can greatly improve radio signal reception, data speeds, bandwidth efficiency and link reliability.

Table of Content

List of Tables

List of Figures

Acronyms and Abbreviations

Abbreviation	Description
AFD	Average Fade Duration
AWGN	Additive White Gaussian Noise
BER	Bit Error Rate
BPSK	Binary Phase Shift Keying
BS	Bit Sequence
ChEst	Channel Estimation
CLK IN	Clock In
CLK	Clock
CP	Cyclic Prefix
CSI	Channel State Information
DC	Direct Current
DSP	Digital Signal Processing
El	Element
ESKOM	Electricity Supply Commission
ET	Eskom Telecommunications
FCC	Federal Communication Commission
FER	Frame Error Rate
FFT	Fast Fourier Transform
GPS	Global Positioning System
HF	High Frequency
HV	High Voltage
ICASA	Independent Communications Authority of South Africa
ICI	Inter Carrier Interference
IEEE	Institute for Electrical and Electronic Engineers
IFFT	Inverse Fast Fourier Transform

INV	Invertor
ISI	Inter-Symbol Interference
ITU	International Telecommunications Union
KVA	Kilo Volt Ampere
LCR	Level Crossing Rate
LF	Low Frequency
LFSR	Linear Feedback Shift Register
LOS	Line of Sight
LPU	Large Power User
LTE	Long Term Evolution
MATLAB	Matrix Laboratory
MIMO	Multiple-In Multiple-Out
ML	Maximum Likelihood
MMI	Man-Machine Interface
M-PSK	M-ary Phase Shift Keying
NRTC	National Rural Telecommunication Cooperative
NRZ	Non-Return to Zero
OFDM	Orthogonal Frequency Division Multiplexing
OSTBC	Orthogonal Space-Time Block Code
PAPR	Peak to Average Power Ratio
PPL	Phase Lock Loop
PRBS	Pseudorandom Binary Sequence
QAM	Quadrature Amplitude Modulation
QPSK	Quadrature Phase Shift Keying
RBG	Random Binary Generator
RF	Radio Frequency
RS	Radio Site
RSS	Receive Signal Strength
RTU	Remote Terminal Unit
RX	Receiver
SCADA	Supervisory Control and Data Acquisition

SISO	Single-In Single-Out
SNR	Signal to Noise Ratio
SS	Substation
STBC	Space-Time Block Code
STC	Space-Time Code
TX	Transmitter
UHF	Ultra-High Frequency
US	United States
USA	United States of America
VHF	Very High Frequency
XOR	Exclusive-OR

Nomenclature

Abbreviation	Description
(*)	Complex Conjugate of the Element
$[\,.\,]^T$	The Hermitian Transpose
$\frac{1}{T}$	Subcarrier Spacing
B_{tot}	Total Number of Bits
E_b/N_0	Energy per Bit to the Spectral Noise Density [Decibels]
F_0	Adjustment Factor
$L_{(v)}$	Knife-edge Diffraction Loss
L_{cable}	Coaxial Cable Loss [Decibels]
$Mb/_S$	Megabits per Second [bits per second]
N_R	Number of Receive Antennas
N_T	Maximum Number of Transmit Antennas
N_r	Number of Receive Antennas
N_s	Number of Time Slots and Rows in the Matrix
N_t	Number of Transmit Antennas
N_t	Number of Transmit Antennas and Column in the Matrix
PL_0	Derived from Empirical Data for Rural Environment
PL_{ee}	Path Loss Lee Model for Irregular Terrain
PL_m	Path Loss in Free Space
R_e	Resistance of the Earth Connection
S_1	Orthogonal Code
S_2	Orthogonal Code
$S_4^c\left(\frac{3}{4}\right)$	Complex Transmission Matrix for 4 Transmit Antennas
S/N	Signal to Noise Ratio [Decibels]
S_n	Data Signal
T_1	Transmitter 1

T_2	Transmitter 2
T_b	Bit Duration
T_{sym}	Symbol Duration
X_k	Data symbols of Complex Numbers
a_0	Random sequence
b/s	Bits per Second
$d_i(t)$	Even Bits (in-phase stream)
$d_k(t)$	Generated Binary Stream
$d_q(t)$	Odd Bits (quadrature stream)
f_c	Centre Frequency
f_d	Maximum Doppler Shift
f_s	Sampling Frequency
ts_1	First Time Slot
ts_2	Second Time Slot
θ_n	Signal Phase
$\in C^{(.)}$	Transmitted Data Signal Energy Complex Matrix
∞	Alfa [Infinity]
B	Channel Bandwidth [Hertz]
C	Total Carrier Power
h	Frequency of the Flat Fading Channel
N	Total Noise Power in the Bandwidth
R	Information Rate [Bits per Second]
BER	Bit Error Rate
C	Channel Capacity [bits per second]
$C(v)$	Pseudorandom Sequence
GHz	Gigahertz
Gr	Receive Antenna Gain [Decibels]
Gt	Transmit Antenna Gain [Decibels]
Hz	Hertz
$I(t)$	Baseband In-phase Signal

KHz	Kilohertz
L	Oversampling Rate
MHz	Megahertz
N	The Maximum Number of the Resolvable Multipath
N	Number of Antennas
N	Number of Subcarriers
Pr	Receive Power [dBm]
Pt	Transmit Power [dBm]
$Q(t)$	Baseband Quadrature Signal
R	Radiation Resistance of the Antenna
$S(t)$	OFDM Symbol Sequence
T	OFDM Symbol Line
THz	Terahertz
W	Bandwidth [Hz]
W	Watts
$X(t)$	Signal with Cyclic Prefix
C	Duty cycle (Random Bit Generator)
C	Duty Cycle [Percentage]
dB	Decibels
dBi	Gain in Decibels Relative to Isotropic
dBm	Power Decibels [milli-watts]
km	Kilometres [km]
m	Meters [m]
ms	Milliseconds [seconds]
$n(t)$	Random Noise
nm	Nano Meter [nm]
$r(t)$	Receive Signal
s	Seconds
s	Transmitted Signal

$s(t)$	Transmit Signal
t	Time
u	The Gain Corresponding to the k^{th} path
y	Output Signal
z	Noise term of Additive White Gaussian Noise (AWGN)
γ	Derived from Empirical Data for Rural Environment
θ	The Phase
μ	Signal Mean
μs	Microseconds [seconds]
μs	Micro Seconds
ρ	Threshold Level Normalised to the root-mean-square
σ	Standard Deviation of the Noise

CHAPTER 1: INTRODUCTION

1.1 Background

The purpose of this dissertation is to develop a low band Very-High Frequency Orthogonal Space - Time Block Code Multiple-In Multiple-Out (VHF OSTBC MIMO) transceiver model to improve the radio signal reception challenges for Eskom along the mountainous Orange River valley of the Northern Cape Province, in South Africa.

The Northern Cape Province is the largest province in South Africa. It occupies 36 million hectares, nearly a third of the countries land area [1]. The Orange River, known to be the longest river south of the Tropic of Capricorn, flows through the province, providing farmers in the area with water resources which are of economic importance in their sector.

The farming communities in the Northern Cape depend on the Orange River for livestock-farming, irrigated cropping, urbanisation and economic development [2]. With this large and intensive agricultural activity which includes crop farming, wool and meat production, comes the use of large amounts of electricity. Therefore, South Africa's supply authority, Eskom, has High Voltage (HV) Substations dotting this area of the Northern Cape, to supply electricity to these farming communities. The agricultural sector is termed a Large Power User (LPU) and is billed by Eskom using the demand charge kilo Volt-Ampere (kVA) tariff bracket.

Eskom uses a system called Supervisory Control and Data Acquisition (SCADA) to both remotely bill customers and to monitor and control its HV equipment such as circuit breakers, transmission lines and transformers in Substations [3].

The region along the Orange River, from Alexander Bay in the South West Coast of Africa, to towns such as Goodhouse, is known for its beautiful Namaqualand landscapes and high mountain ranges. The area boasts mountains as high as 1258m above sea-level [4]. However, because of the high mountain ranges in the area, all forms of radio and cell phone communication are unavailable along the Orange River where one of Eskom's HV Substation is located.

Due to obstructions to radio signals caused by the high mountains [5], the SCADA service which monitors Eskom's HV equipment is also unavailable.

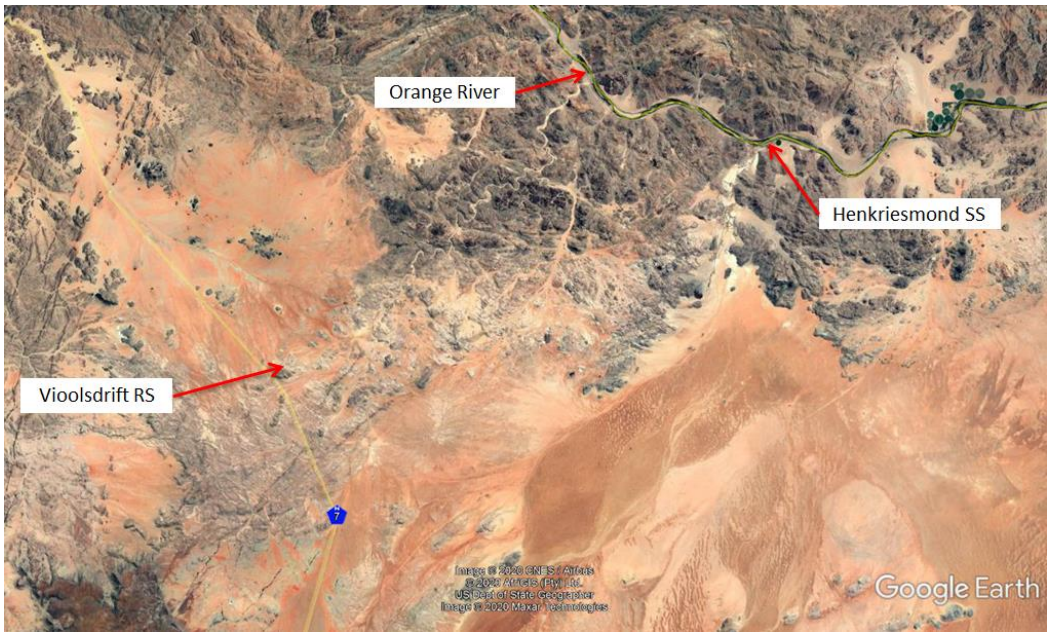

Figure 1. 1: Mountainous Terrain in the Northern Cape Province, South Africa

The terrain of the area of interest (Between Vioolsdrift Radio Site and Henkriesmond Substation) has been extracted from Google Earth, as shown in Figure 1.1. The image from Google Earth is imported to Atoll Wireless Network software to obtain a coverage plot diagram of the area, as shown in Figure 1.2.

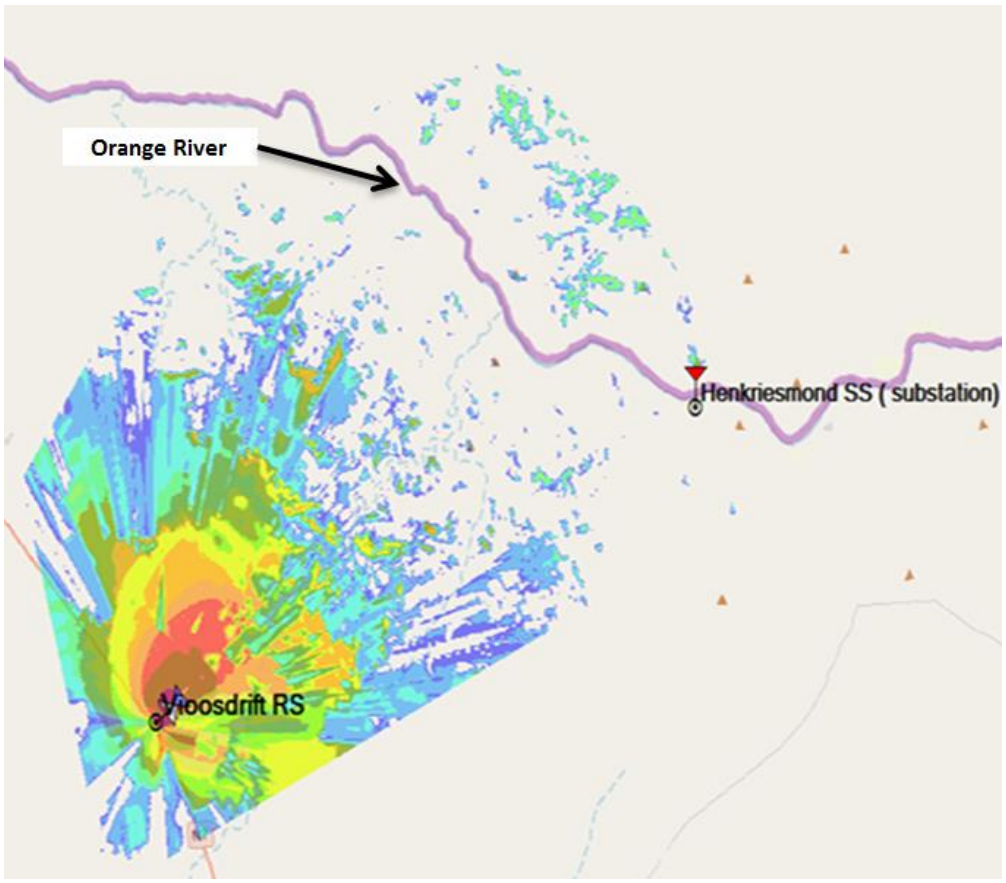

Figure 1. 2: Atoll Wireless Coverage Plot Diagram

In Figure 1.2, the Ultra-High Frequency (UHF) radio signals transmitted from the Eskom Radio Site-Vioolsdrift towards Henkriesmond Substation are reflected by the mountainous terrain [5], thus rendering the Orange River valley where Henkriesmond Substation is, void of radio signals. This implies that the SCADA service will not be available in this region under these conditions.

In the area under investigation, the Vioolsdrift Radio Site lies at 870m above sea-level, while Henkriesmond Substation lies at 208m above sea-level. The two sites are 32.8km apart, with uneven terrain in-between. Figure 1.3 is a Line of Sight (LOS) diagram showing a non-line of sight condition between Vioolsdrift Radio Site and Henkriesmond Substation.

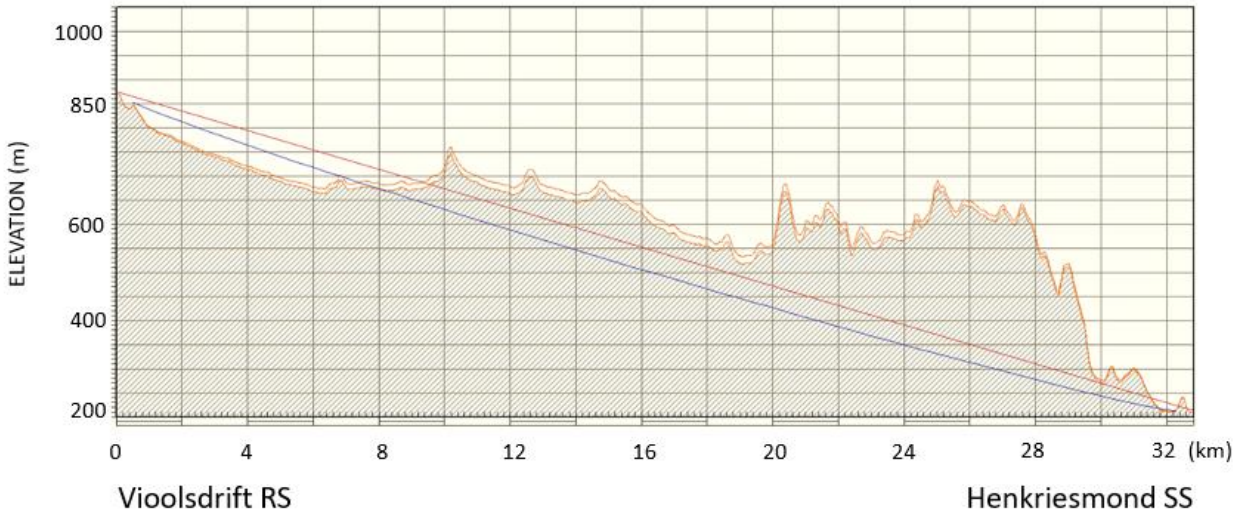

Figure 1. 3: Line of Sight Diagram

The high mountain peaks between the two sites make radio communication impossible. As evident in Figure 1.4, the multipath radio signals are reflected off the mountainous terrain and lost in the medium, resulting in signal loss. The expression for Path loss is the difference between the transmitted signal and the received signal power [6]. The Lee model is a path loss model used in irregular terrain with diffraction loss [7]. It is expressed by the following equation:

$$PL_{Lee} = PL_0 + \gamma \log_{10}(d) + F_0 + L_{(v)} \quad (1.1)$$

Where:

PL_0 and γ = derived from empirical data, e.g. PL_0 = 89 and γ = 43:5 for rural environment

F_0 = Adjustment factor.

$L_{(v)}$ = Knife-edge diffraction loss.

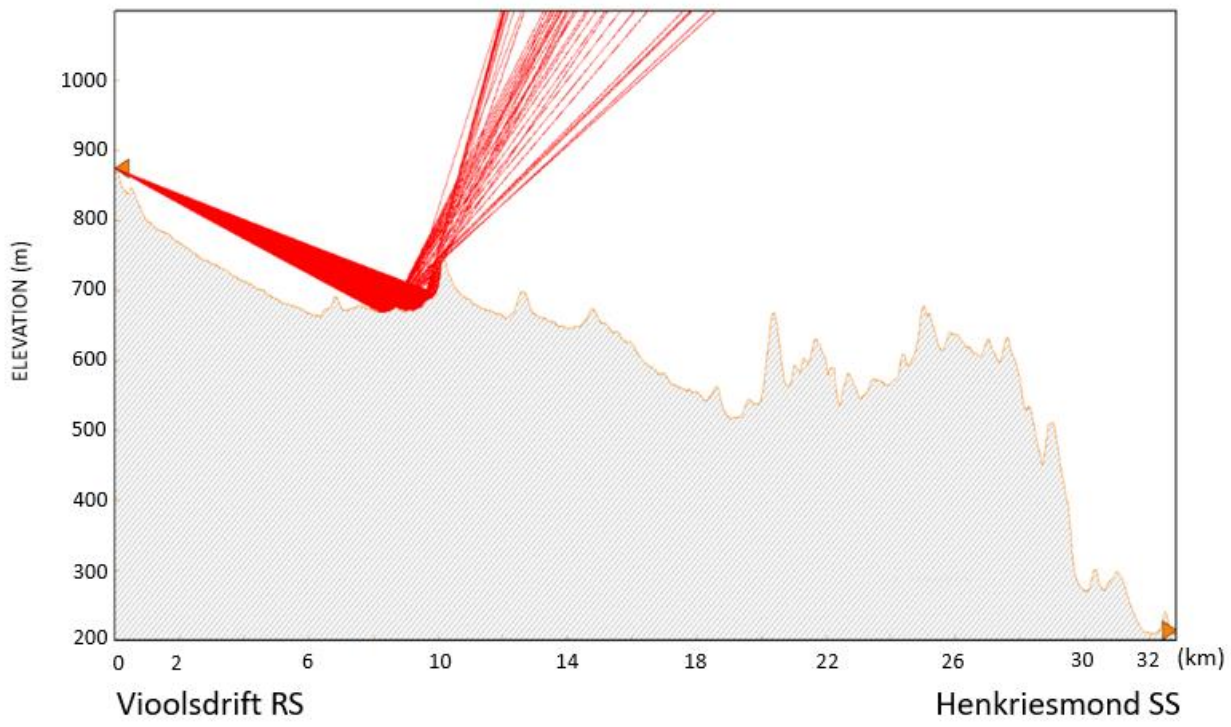

Figure 1. 4: Multipath Propagation Diagram

Table 1.1 illustrates the performance results of the existing Eskom radio link, using Pathloss 4 software, in the area of concern. As seen in Table 1.1, the effects of the mountain can be observed at the 9km mark towards the Henkriesmond Substation (Figure 1.4), where the path losses increase significantly due to reflection of the radio signals by the mountain, with net path loss at 157.07 dB.

TABLE 1. 1: LINK PERFORMANCE OF THE EXISTING ESKOM RADIO LINK

Parameters	**Vioolsdrift RS (TX)**	**Henkriesmond SS (RX)**
Effective Radiated Power (Watts)	12.13	7.92
Effective Radiated Power (dBm)	40.84	38.99
Free Space Loss (dB)	115.19	115.19
Polarization	Vertical	Vertical
Net Path Loss (dB)	160.74	157.07
RX Signal (dBm)	-123.75	-120.08
Fade Margin (dB)	-16.75	-13.08

1.2 Problem Statement

The unavailability of a radio communication link in this particular mountainous region means no remote monitoring of the Eskom HV Network by SCADA. As shown in section 1.1, the high mountain peaks near the farming town of Goodhouse next to the Orange River in the Northern Cape greatly compromises radio communication in the area. This is so because higher frequency radio signals have smaller wavelengths and are susceptible to attenuation due to obstructions such as high mountains or tall buildings [8]. This is a major setback for Eskom because without the 24-hour remote monitoring of its HV assets by the SCADA system, the following may result:

- Prolonged outages without Eskom's knowledge.
- Poor service to customers.
- Loss of revenue due to Eskom.
- The dispatch of Eskom personnel each time there is a fault condition or a need to read customer meter points.
- Time lost due to travelling to remote sites.
- Vandalism of HV plants.
- Danger to HV equipment, the environment and human life.

Without remote monitoring of HV plants by the SCADA system, as is the case in the area of concern in the Northern Cape Province, Eskom's electricity network is compromised.

1.3 Objectives of the Study

The objective of this quantitative study is to develop a low band Very High Frequency- Orthogonal Space Time Block Code, Multiple-In Multiple-Out (VHF-OSTBC MIMO) simulation model that addresses the problem identified in section 1.2.

High mountains obstruct high frequency radio signals (300MHz -∞), thus causing multipath fading and poor radio link performance [9]. However, according to [10, 11, 12], frequencies at lower bands (3-30 MHz) can travel longer distances with lower attenuation levels and can easily diffract over large obstacles such as mountains. Applying this knowledge, the objectives of this study are:

- To exploits the low VHF frequency band at 70MHz to achieve diffraction.
- To develop a Rayleigh fading channel with Added White Gaussian Noise (AWGN) to model a non-line of sight noisy channel.
- To apply the OSTBC MIMO transceiver model to achieve greater channel capacity, reduced the Bit Error Rate (BER) and interference.
- To improve Signal to Noise Ratio (SNR) and increase the chances of radio signal reception at the Orange River valley.

1.4 Research Methodology

To achieve the above-mentioned objectives the following methodology is applied:

- Literature Review: Existing literature related to factors affecting radio signal propagation and the unique characteristics of the low frequency band; the MIMO OSTBC technology and its application in irregular terrain environment was reviewed; and the conclusion drawn on the literature found.
- System Model Development: After studying the operation of the different sections of the proposed model, a mathematical model for an OSTBC MIMO transceiver applied to a Rayleigh Fading channel with Added White Gaussian Noise (AWGN) employing a 4x4 MIMO system was developed
- Simulations: After developing the mathematical model, a low band VHF OSTBC MIMO model was developed and applied in Matlab/Simulink software. The behavior of the model was analysed and the results of the radio link performance discussed.

1.5 Hypothesis

The modelled VHF OSTBC MIMO transceiver system significantly reduces the BER and interference hence improving the performance of the radio link. The use of multiple antennas on both ends of the radio link creates spatial diversity which increases the chances of the original signal strongly recovered at the receiver. The VHF portion of the system achieves diffraction over the high mountains for the reception of the radio signal at the receiver.

1.6 Limitations of the Study

This study is limited to the development of an OSTBC MIMO transceiver system model by employing four different MIMO antenna arrays, with Added White Gaussian Noise (AWGN) in a Rayleigh Fading channel in Simulink. A coded Matlab script, simulating a VHF OSTBC MIMO radio coverage prediction employing three different low VHF frequency bands is developed. The study is based on simulations. Experiments on a prototype are beyond the scope of this work.

1.7 Contribution to Knowledge

This study presents a review of radio frequency (RF) propagation challenges over irregular terrains and MIMO system principles to mitigate these challenges. Although the MIMO system has been exploited widely for many years especially in the cellular phone environment, its application in the low VHF band (49-108 MHz) for SCADA purposes has not been widely investigated, as has been in this study. Furthermore, the application of the OSTBC MIMO technology in the low VHF frequency band for improvement of signal reception in irregular terrain has certainly not been explored in the mountainous regions of the Northern Cape Province in South Africa. Therefore, this study encourages further research into the use of the VHF OSTBC MIMO systems to improve radio communication in mountainous terrains. Moreover, the information provided in this study not only presents useful information for radio engineers designing and installing radio systems in mountainous areas, but also for the Eskom business to improve revenue, provide quality service to the customer and to improve the safety of the equipment and personnel in the workplace. Further

work involving testing this technique in the field using real data is planned at Eskom in the future to improve its radio communication.

1.8 Publications during the Study

Conference Papers:

X. B. Maxama and E. D. Markus, "A Survey on Propagation Challenges in Wireless Communication Networks over Irregular Terrains", IEEE Open Innovation Conference, Johannesburg, South Africa, Oct 2018.

X. B. Maxama and E. D. Markus, "VHF OSTBC MIMO System Used to Overcome the Effects of Irregular Terrain on Radio Signals," The Fourth International Conference on Computing and Network Communications (CoCoNet'20) Conference, Chennai, India on October 14-17, 2020.

1.9 Dissertation Layout

Chapter 1 is the introduction to this dissertation. It presents a background on the SCADA service at Eskom and the radio signal propagation challenge in a mountainous area of the Northern Cape Province. It lists the problem statement, objectives, methodology, hypothesis, delimitation of the study, as well as the research outputs.

Chapter 2 presents an overview of literature on radio signal in various propagation environments with a focus on irregular terrain; technologies used in such environments and their general advantages and disadvantages. The primary focus is on a review of the OSTBC MIMO technology, its principles, and applications.

Chapter 3 focuses on the development of the mathematical model for an OSTBC MIMO transceiver system with Added White Gaussian Noise (AWGN) in a Rayleigh Fading channel. The model is developed using the Matlab/Simulink software.

Chapter 4 displays the simulation results of the developed OSTBC MIMO model and the performance results of a proposed VHF OSTBC MIMO transceiver system in the area of concern in the Northern Cape Province.

Chapter 5 presents the conclusion and suggestions for future research to be carried out in the area of radio propagation in mountainous areas.

CHAPTER 2: LITERATURE REVIEW

2.1 Introduction

This chapter presents a review of different factors affecting wireless communication over different propagation environments, with a focus on irregular terrain. Besides, some methods to mitigate these factors are mentioned. It also presents recent developmental studies focusing on technologies such as the MIMO technology to efficiently improve communication in irregular terrain.
The different mechanisms that affect radio link performance in wireless communication over irregular terrain have been identified to be reflection, diffraction, scattering and multipath fading [13]. These mechanisms weaken the radio signal strength thus causing path loss.

2.1.1 Path Loss

Path loss, which is known in telecommunication systems as the difference between the transmitted signal and the received signal power is expressed by the following equation in Free-Space:

$$PL_m = Pt - \mathrm{Pr} + Gt + Gr - L_{cable} \quad (2.1)$$

Where:

$Pt =$ Transmit power (dBm).

Pr = Receive power (dBm).

$Gt =$ Transmit antenna gain (dB).

$Gr =$ Receive antenna gain (dB).

L_{cable} = Coaxial cable loss (dB).

Authors in [14] have further maintained that the distance between the transmitter and receiver, the frequency used, the antenna height and the terrain shape may also contribute to path loss. For instance, according to [15], for any given radio propagation environment, the radio signal strength

loss increases in proportion to the increase in the distance between the transmitter and receiver. Figure 2.1 illustrates that path loss increases exponentially as the distance between the transmitter and the receiver increases.

In [16], the authors discuss how different propagation environments and distance can seriously influence the increase in path loss. They confirm that signal loss increases in non-line of sight irregular terrain environments than in free space. The report in [16] also indicates that different propagation terrains render different path loss exponent values. For instance, the path loss exponent value for free space is 2, while the value for irregular terrain would be in the region between 3.5 and 4.2. Therefore, from the findings in the report, we do realise that path loss is greater in irregular terrain environments.

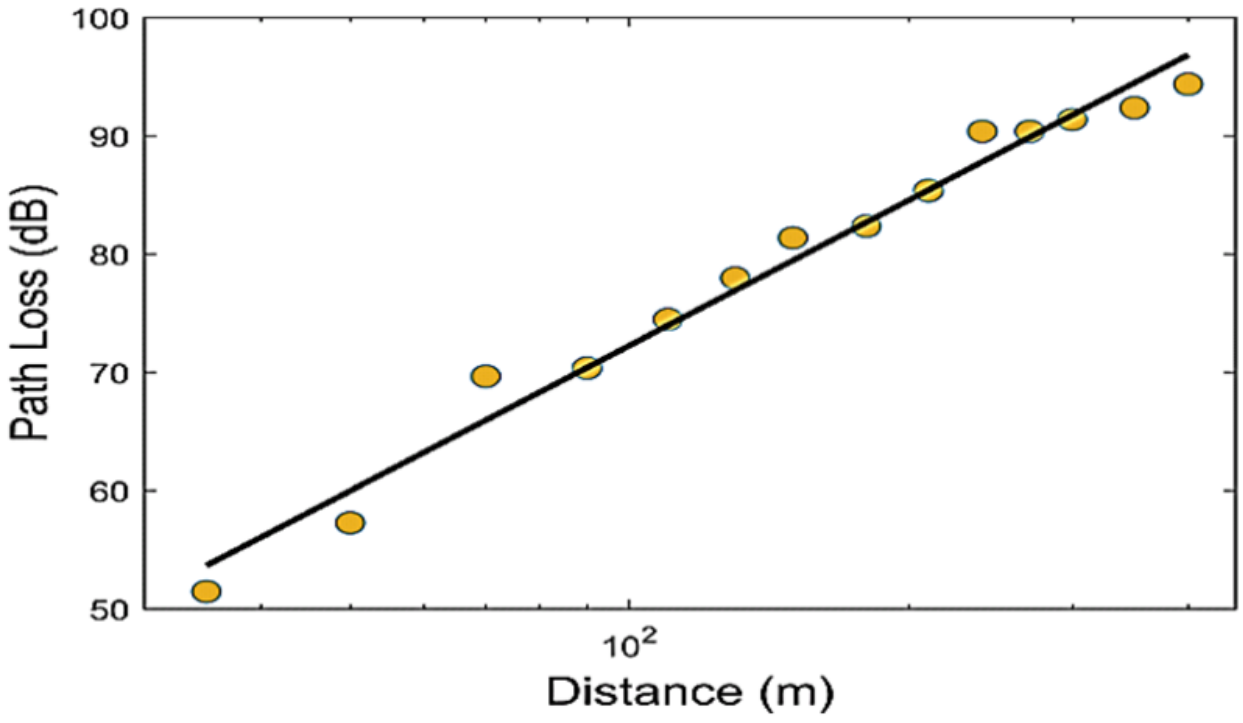

Figure 2. 1: Path loss vs. Distance [16]

2.1.2 Multipath Fading

Fading has always been looked at as a great challenge in the radio engineering field. When radio signals arrive at the receiver by two or more delayed paths, fading occurs. This causes the signal strength at the receiver to vary due to amplitude and phase shifts [18]. However, many researchers on multiple antenna arrays have discovered that multipath fading can be a positive especially in Multiple-In Multiple-Out (MIMO) applications [19]. MIMO technology takes advantage of multipath propagation and exploits it for its spatial diversity feature to improve Signal to Noise Ratio (SNR).

2.1.3 Radio Frequencies

The type of radio frequency band used can be a factor in the successful transmission of radio signals. Obstructions such as mountains or tall building appear very large, in the way of microWaves and millimetre Wave frequencies, whose wavelengths are very small, thus resulting in the reflection and attenuation of the transmitted signal [8]. Figure 2.2 illustrates how the small wavelengths of high frequencies are susceptible to attenuation due to environmental factors and uneven terrain [11].

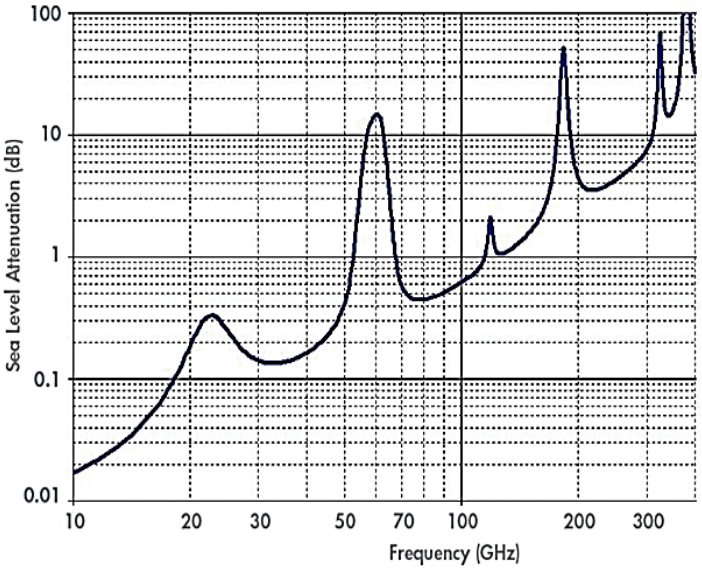

Figure 2. 2: Higher Frequencies are Susceptible to Attenuation Due to Obstructions [11]

- High Frequency Band

High frequencies in a radio link usually operate by line of sight (LOS), thus the transmitting and receiving antenna path has to be clear of obstructions, otherwise chances of signal attenuation will be higher [20]. The author in [22] also concurs with the fact that high frequency signals easily get reflected by irregular terrain such as high mountains and tall buildings. According to [8], this is possible because high frequencies have short wavelengths of up to (1 to 10 mm). Therefore, when they come into contact with a large object such as a mountain, they are reflected and attenuated [11].

TABLE 2. 1: FREQUENCIES AND THEIR RESPECTIVE WAVELENGTHS

Frequencies	**Wavelengths**
50-60 Hz	6000-5000 km
3-30 KHz	100-10km
30-300KHz	10-1km
180-1600KHz	1.7km-188m
1.8-30 MHz	167-10m
88-108 MHz	3.4-2.7m
300-3000MHz	1-0.1m
800-2200MHz	0.375-0.136m
1-60 GHz	0.3-0.005m
60-300 GHz	0.005-0.001m
352,230,193 THz	1550,1300,850nm
420-750 THz	714-400nm

- Low Frequency Band

As illustrated in Table 2.1, the Low Frequency (LF) band which is between (30–300 kHz), has longer wavelengths of up to (1 to 10km) and can be transmitted over long distances with low attenuation levels. These frequencies according to [11, 22, and 23] easily diffract over large obstructions such as mountains. This attribute of the LF band has attracted the attention of this

research and has influenced the search for a suitable transceiver system to exploit it with. However, the drawback of the LF band is low data rates and a small bandwidth of 20 to 150 Hz [23]. This frequency band is also susceptible to noise [24].

2.1.4 Interference

Studies reveal that objects in the propagation path such as magnetic fields from high voltage electricity lines, moving vehicles and phenomenon such as thunderstorms and atmospheric noise play a part in radio signal interference [15 and 25]. Radio signal interference could also be caused by the following:

- Co-channel and Adjacent Channel Interference:

Interference can possibly be generated within a propagation channel by a co-channel and adjacent channel interference. Co-channel interference is generated when two frequency channels are close to each other, using the same frequency band. Adjacent channel interference occurs when stray signals from a nearby transmitter creep into the receiver. These may be resolved by increasing distance between the channels or good filtering [18].

- Electromagnetic Interference:

According to a report in [25], some industries are unwilling to utilise wireless communication in their work environment because of reliability issues. In industrial environments, factors such as metallic structures, electric motors and repair work are sources of electromagnetic interference and could cause radio signal degradation. These radio signal challenges could negatively impact the reliability of communication, thus increasing risk to equipment and personnel in the workplace.

- Solar Radiation:

Radiation from the sun is another source of interference, radio signals could suffer from. The ionosphere can at times be disturbed by solar flares which give off electromagnetic radiations that may impact radio signals. Solar flares create increased ionization in the lower ionosphere, which causes phase shifts in the LF band and increased fading in HF and VHF bands and cause

interference. During ionospheric disturbances, applications such as the Global Positioning System (GPS) may be affected [26].

2.1.5 Signal Loss due to Environmental Factors

- Rain:

In [14 and 15], the authors discuss the impact of ambient temperature, haze, dust, snow and other forms of precipitation have on the attenuation of a high frequency transmitted signal. Heavy rainfalls also can lead to distortion of the radio signal, especially in frequencies above 10 GHz [27].

- Fire:

A study done in Australia where fires are likely to start showed that during fire conditions and heavy smoke, radio communication at ground level deteriorated [28].

- Vegetation:

Vegetation and trees also cause radio signal losses at frequencies up to 10 GHz. Trees have an absorbing effect on radio signals mainly for propagation over the trees [29].

- Ground Temperature:

UHF and VHF radio signals are also reflected by large objects and absorbed by some environmental factors such as humidity, ground temperature, and vegetation. When there is an increase in ground temperature in the propagation path, there will be a weakening of the radio signal [15].

- Ambient Temperature:

The results found in [27] showed that variations in weather conditions affect the received signal strength. When the ambient temperature rises, the signal strength drops and vice versa. In summer, the signal strength drops during the day and rises during the night. In winter the signal strength increases [27].

2.1.6 Antenna Height

- Ground Conductivity and Ground Humidity:

The High Frequency (HF) band is more likely to be degraded by humidity in the ground than the Low Frequency (LF) band. Permittivity and conductivity in the ground increase when the ground is moist. Conductivity becomes even higher if the moisture in the ground is salty e.g. seawater [15]. The effect of the ground on a transmitted radio signal is astounding. The US Army Signal Center and Fort Gordon [15], conducted a study wherein they discovered that when an antenna transmits a radio signal closer to ground, a voltage becomes induced in the ground. The induced voltage in the ground, in turn, reduces the power of the transmitted signal, thus degrading the radio signal as it is propagated.

However, the radio signal degradation caused by the induced voltage is dependent on the ground's electrical properties [15]. If the ground has good conductivity, then there will be less attenuation and better propagation of the signal. Also, according to [15], a radiating antenna that is closer to the ground acts as a capacitor, where the energy is stored. The interaction between the antenna and the ground creates an impedance. This impedance increases attenuation relative to the ground's conductivity. The radiation pattern of an antenna can be impacted by the ground. Horizontally polarised antennas' radiation pattern is dependent on the antenna's height above the ground. Vertically polarized antennas' radiation pattern is dependent on the conductivity of the ground and also on the height of the antenna above the ground. The radiation efficiency of an antenna near ground is determined by the following equation:

$$Antenna\ Efficiency = \frac{R}{R + R_e} \qquad (2.2)$$

Where:

$R =$ Radiation resistance of the antenna.

$R_e =$ Resistance of the earth connection.

Studies show that sufficient antenna height above the ground, the right polarization and ground conductivity have an enormous impact on radio signal propagation [8]. A dry and sandy terrain will experience an increase in signal loss [15]. According to [10], an alternative way to increase

ground conductivity immediately around the antenna, in dry terrain environments, is to either plant a 2m long copper rod into the ground or conceal metal sheets into the ground.

2.2 Methods to Mitigate Propagation Challenges in Irregular Terrain

This section has categorised methods used previously to combat radio signal propagation challenges in irregular terrain. Different modulation schemes and propagation methods in a Rayleigh fading channel are cited with their advantages and disadvantages in Table 2.2.

TABLE 2. 2: METHODS USED TO MITIGATE WIRELESS COMMUNICATION CHALLENGES IN IRREGULAR TERRAIN

Method	Description	General advantages	General disadvantages	Typical application in wireless communications
Groundwave propagation.	LF band propagation along the surface of the ground.	Signals travel long distances. Low attenuation. Diffracts over obstacles.	Very large antennas. Antenna height high. Signal affected by ground conductivity. Limited working bandwidth. Susceptible to noise [32].	Long distance communications. Mountainous area [22].
Sky-wave propagation.	HF band propagation that uses the Ionosphere.	Signals travel long distances. Supporting structures for long distance communication not necessary. Uses Ionosphere to propagate radio signals.	Very large antennas. Limited working bandwidth. Susceptible to noise [33].	It is used in disaster relief communications. Long distance communications [34].
MIMO (Multiple-In Multiple-Out)	It is a transceiver which uses multiple antennas at	It exploits multipath propagation to improve signal reception.	In the market it is currently available in microwave and UHF frequency applications.	Largely used in telecommunication environments where there is heavy fading [19].

	the transmitter and receiver.	It creates spatial diversity which increases the chances of the original signal being largely recovered at the receiver. It improves SNR and link performance [19]. Increased channel capacity. Overcomes fading. Effective in helping to reduce the impact of time dispersion, path loss and interference [17].		
OFDM (Orthogonal Frequency Division Multiplexing	It is a modulation technique that divides the bandwidth into parallel multi-narrow band carriers to increase data rates [30].	Increases data rates. Prevents inter-symbol interference (ISI) caused by multipath delay in the medium [31, 34]. It improves spectral efficiency and solves multipath propagation problems [35]. It improves SNR [36].	It has noisy amplitude with a large range. It requires RF power amplifiers with high peak to average power ratio. It is sensitive to Doppler shift. It suffers loss of efficiency caused by cyclic prefix [65].	It is used as a modulation technique in MIMO systems [65].
(HF) band coupled with a discone resonant antenna.	This is the HF band at (20-30 MHz) using a discone antenna to	Lower transmission power levels. Low background noise.	Large Antennas. Noise. Low data rates. Limited working bandwidth.	Groundwave communication which is a transmission mode suitable for areas where radio

	achieve groundwave propagation [37].	Desired groundwave propagation [37]. Groundwave signals diffracts around objects such as mountains. Groundwaves propagate in the area between the ground and the air for short distances of up to 100 km over land and 300 km over sea [38].	Susceptible to noise [33].	communication is unavailable due to mountainous terrain [39].
HF MIMO OFDM	It is a transceiver system combining MIMO and OFDM operating in the HF band.	Improved noise reduction Increased bandwidth utility at HF band. Increased data rates [40].	Large antennas. High cost. Suffers from poor power efficiency. Requires RF power amplifiers with a high PAPR.[69]	According to [34], this technique works well in irregular terrain environments.

Table 2.2 presents an overview of various methods that have been used over the years to mitigate the negative impact of radio signal propagation in irregular terrain. It further indicates the advantages and disadvantages experienced in employing each technique. It is evident from the literature presented that wireless communication challenges over irregular terrain have long been a serious concern for radio engineers, based on the studies and technologies developed in the past to try to eradicate it. However, the large demand for wireless communication technologies that work over irregular terrain, still exist in many countries across the world. In view of this, this study is being conducted. Of particular interest in this study, and which seems not to have been researched much by the different authors cited, is the MIMO technology operating in the low VHF band. This study seeks to exploit the MIMO technology together with the OSTBC scheme operating at in the low VHF band to cater for the SCADA service in the South African context.

Coupling these systems could be a solution to the wireless communication challenges in irregular terrain for Eskom SCADA in the Northern Cape Province.

2.3 SCADA System

The SCADA is a computer-based system which provides real-time management of the electricity network. It enables a system controller to continuously monitor, collect data from and control remote High Voltage (HV) equipment via the Telecommunications Radio network [3]. The SCADA system saves the Eskom business time and costs by removing the need to dispatch personnel to site each time an inspection, collection of data or a manual reset needs to be performed. Real-time monitoring, network fault detection, automated commands, billing, archiving of events, measurements, historical reporting, remote meter reading capacity and data collection are some of the functions of the SCADA system.

In Eskom, the SCADA system is mainly employed for the following functions:

- Management and control of Power Generation
- Management and control of Transmission and Distribution electrical networks

The remotely collected data and alarms in a SCADA system are monitored on a Man-Machine Interface (MMI), which is a computer located at a control centre as depicted in Figure 2.3. In the event of a fault, the SCADA master detects the location of the fault via a Remote Terminal Unit (RTU) and displays the fault condition on the MMI so that the system controller may be able to identify it and resolve it timeously. Automated commands may also be sent in the system, for the purpose of controlling remote HV equipment. Measured analogue values such as voltage, current and frequency can also be displayed on the MMI from remote sites.

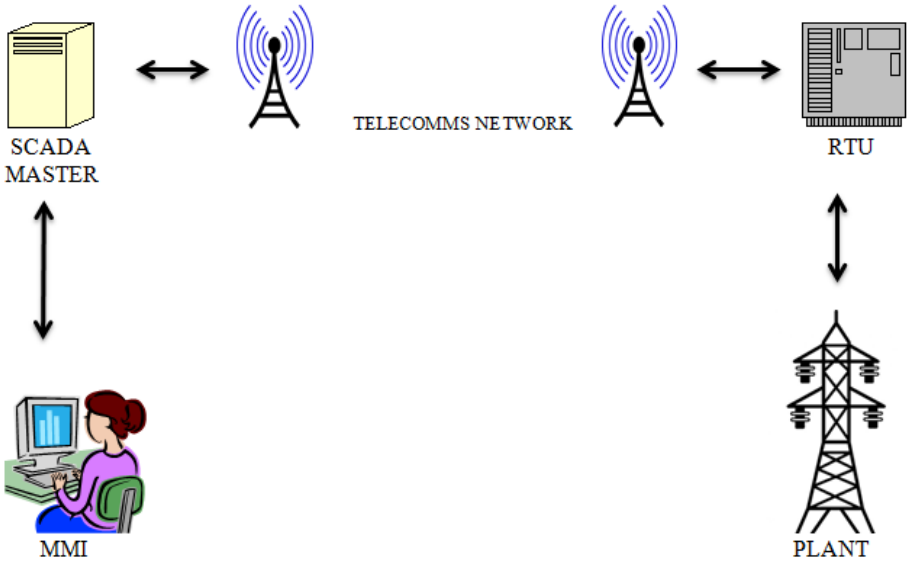

Figure 2. 3: SCADA System Architecture

2.4 Orthogonal Frequency Division Multiplexing (OFDM)

According to [41], Orthogonal Frequency Division Multiplexing (OFDM) modulation technique has been known since the 1960s; however, its extensive use is only recent. OFDM technology provides higher data rates and increased bandwidth efficiency at no extra transmit power or bandwidth [41, 42]. OFDM divides the signal into several parallel-narrow band carriers in the same bandwidth [43]. These carriers are orthogonally modulated with information using various modulation schemes at lower data rates (e.g. BPSK, QPSK or 4-QAM). Figure 2.4 illustrates 8 orthogonal subcarriers each at amplitude 1 in the same bandwidth.

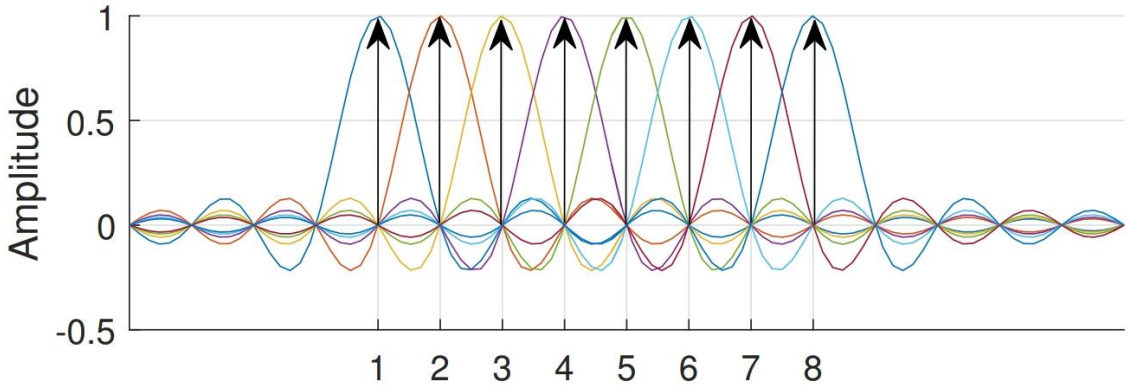

Figure 2. 4: OFDM Subcarriers in Frequency Domain [49]

Transmitting multi-data streams in the same bandwidth increases the data rate [44]. The parallel narrow bands are independent of each other therefore Inter-Carrier Interference (ICI) is prevented. These narrow bands are then fed to a Cyclic Prefix (CP) or guard interval to prevent Inter-Symbol Interference (ISI) caused by multipath delay in the medium [41, 45]. At the receiver, the data signals are sampled at longer symbol periods to recover much of the data [43].

The OFDM technique has shown to improve spectral efficiency and solves multipath propagation problems [46]. The different data streams from different multiple paths are combined at the receiver using special algorithms to strengthen them, thus improving SNR [47]. To increase the signal coverage area, throughput and spectral efficiency, advanced antenna technology such as MIMO is used together with OFDM modulation technique [69]. Equation (2.3) is a low pass equivalent of the OFDM signal is expressed as:

$$X(t) = \sum_{k=0}^{N=1} X_k \; e^{j2\pi kt/T} \qquad , 0 \leq t < T \tag{2.3}$$

Where,

X_k = Data symbols of complex numbers representing BPSK, QPSK or QAM.

N = Number of subcarriers.

T = OFDM symbol line.

$\frac{1}{T}$ = Subcarrier spacing.

The OFDM symbol sequence is represented by the following equation:

$$S(t) = \sum_{k=-\infty}^{+\infty} X(t - kT) \quad (2.4)$$

To counter ISI, a guard interval of length T_g is placed in front of the OFDM block. During this time interval, a cyclic prefix is transmitted. Thus, the signal with the cyclic prefix included is given by [69]:

$$X(t) = \sum_{k=0}^{N=1} X_k \; e^{j2\pi kt/T} \quad , -T_g \leq t < T \quad (2.5)$$

The Inverse Fast Fourier Transform (IFFT) and Fast Fourier Transform (FFT) are the modulation and demodulation methods used in OFDM.

2.5 Multiple-In Multiple-Out (MIMO) Technology

Wireless communication channels suffer from severe attenuation due to fading and interference, which distorts the received data signal [51]. According to [52], when this transpires, the signal may experience reflection, refraction and superposition resulting in inter-symbol interference (ISI) caused by multiple copies of the original signal arriving at the receiver at different time periods. This makes it difficult for the receiver to recover the originally sent data unless the receiver is configured to provide some form of diversity. Many studies recommend diversity to be the most efficient method to combat multi-path fading and interference [53, 54 and 55]. In most applications, diversity is achieved by employing antenna arrays at both the transmitter and receiver [56]. First discovered in the mid-1990s [57], the Multiple-In Multiple-Out (MIMO) technology is a transceiver which makes use of multiple antennas at both the transmitter and receiver [58]. The use of a multiple antenna transceiver in MIMO achieves spatial diversity, where the multiple copies of the transmitted signal take multiple paths to the receiver and are recovered using Digital Signal Processing (DSP) techniques, at different times and phases [59]. Figure 2.5 is a MIMO block diagram employing two antennas at both the transmitter and receiver. The MIMO system

provides many features such as beamforming, diversity coding and spatial multiplexing. The following features not only help enhance the performance of the wireless communication link but are what make MIMO unique [19].

- Beamforming is a technique where the same signal is transmitted with a different phase and gain over the multiple transmit antennas so that the received signal is saturated with the originally sent data.
- Diversity assists with sending a single data stream via all transmit antennas.
- Spatial multiplexing increases capacity by dividing a high rate bandwidth into small multiple low rate streams and transmitting them via multiple antennas thus increasing data rates with less power and without additional bandwidth.
- Compatibility with Spate-Time coding techniques such as OSTBC to increase the probability of recovering data exponentially.

The use of the MIMO technology increases capacity, combats the effects of frequency selective fading, reduces bit error rates and improves Signal to Noise Ratio (SNR) [60 and 61].

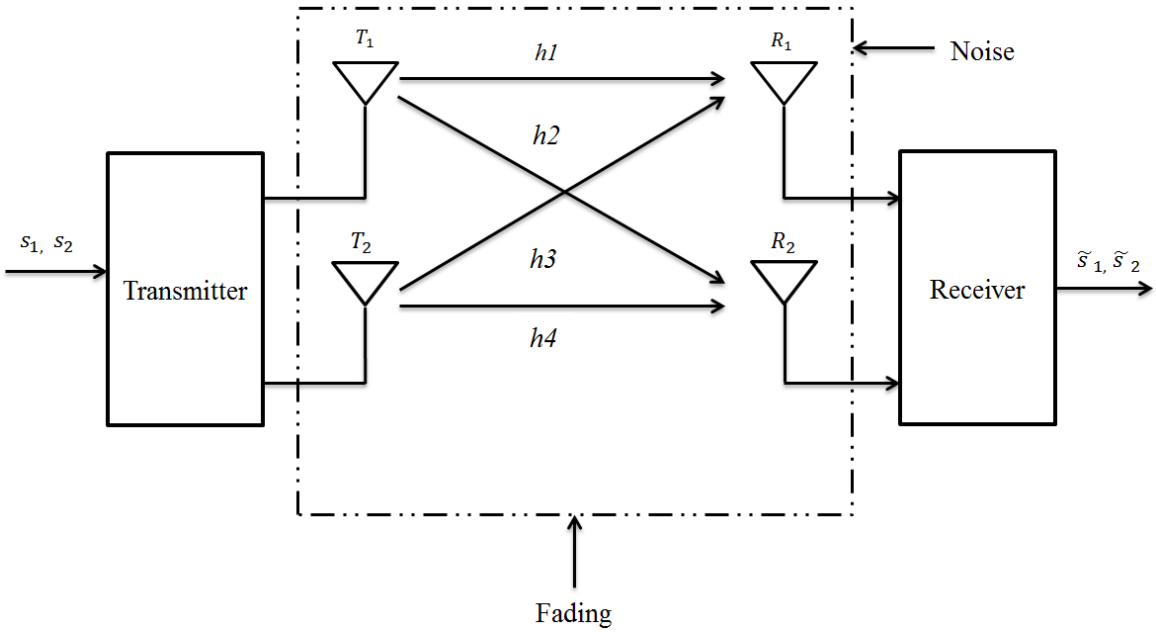

Figure 2. 5: MIMO System Block Diagram

Theoretically, MIMO systems render increased capacity that can increase linearly with the number of antennas used [52]. Applying Shannon's Law which governs the amount of data that is sent through a channel in the presence of noise, this theory can be confirmed. The following is Shannon's Law equation:

$$C = W \log_2(1 + {}^{S}/_{N}) \quad (2.6)$$

Where:

C = Channel capacity in bits per second (b/s).

W = Bandwidth in Hertz (Hz).

${}^{S}/_{N}$ = Signal to Noise Ratio in decibels (dB).

With the use of the MIMO technology, the capacity of the channel increases as the number of antennas used increase. This theory is confirmed by the following equation:

$$C = NW \log_2(1 + {}^{S}/_{N}) \quad (2.7)$$

Where:

N = Number of antennas used.

An increase in the number of antennas used in the system, results in greater the channel capacity [20].

2.6 Orthogonal Space Time Coding (OSTBC) Technology

MIMO systems can enhance channel capacity by using spatial multiplexing. However, to achieve enhanced channel reliability orthogonal space-time coding is used (OSTBC) [52]. The ultimate goal for employing OSTBC is to achieve full diversity, increased capacity and reduced bit errors. Space-time trellis coding combines signals at the receiver with coding methods suitable for multiple transmit antennas. Certain space-time trellis codes which are made for two to four

antennas perform well in slow fading environments. However, its decoding is complex and increases with the transmission rate [56].

Alamouti [62], in resolving the decoding problem in space-time trellis codes came up with a coding scheme using two transmitting antennas. Alamouti's coding scheme namely, space-time block codes (STBC), introduced the maximum likelihood (ML) technique which is less-complex and simplifies the receiver [52]. The Alamouti code is described by the following matrix:

$$S_n = \begin{bmatrix} S_1 & S_2 \\ -S_2^* & S_1^* \end{bmatrix} \tag{2.8}$$

Where:

S_n = Transmit data matrix.

$S_1, S_2, -S_2^*, S_1^*$ = Data symbols.

The code uses two transmitting antennas T_1 and T_2, a modulation scheme that maps the bits into one symbol, with $M = 2^m$, that is it will transmit 2 symbols every 2-time intervals. Examples of those modulations schemes are Quadrature Phase Shift Keying (QPSK) and Quadrature Amplitude Modulation (QAM). In this coding scheme, the first antenna T_1 transmits the symbol S_1 in the first time slot ts_1. Also, within the first time slot ts_1, the second transmitter T_2, transmits the symbol S_2. In the second time slot ts_2, the respective transmitters T_1 and T_2transmit symbols $-S_2^*$ and S_1^* simultaneously [63].

Tarokh [56], took Alamouti's work further to produce orthogonal space-time block codes (OSTBC) for more than two transmit antennas. Researchers have examined Tarokh's STBCs and achieved a maximum Signal-to-Noise Ratio at the receiver [64]. For OSTBC, Tarokh designed blocks with ½ and ¾ code rates and full diversity.

Equation (2.9) is a Tarokh's complex transmission matrix achieving full diversity for four transmit antennas [65]:

$$S_4^c\left(\frac{3}{4}\right)=\begin{bmatrix} S_1 & S_2 & \frac{s_3}{\sqrt{2}} & \frac{s_3}{\sqrt{2}} \\ -S_2^* & S_1^* & \frac{s_3}{\sqrt{2}} & \frac{-s_3}{\sqrt{2}} \\ \frac{s_3^*}{\sqrt{2}} & \frac{s_3^*}{\sqrt{2}} & \frac{-s_1-s_1^*+s_2-s_2^*}{2} & \frac{-s_2-s_2^*+s_1-s_1^*}{2} \\ \frac{s_3}{\sqrt{2}} & -\frac{s_3}{\sqrt{2}} & \frac{-s_2-s_2^*+s_1-s_1^*}{2} & -\frac{s_1-s_1^*+s_2-s_2^*}{2} \end{bmatrix} \quad (2.9)$$

Where:

(*) = Complex conjugate of the element.

$S_4^c\left(\frac{3}{4}\right)$ = Matrix code for complex transmission matrix for four transmit antennas.

2.7 The low Very High Frequency (VHF) Band in SCADA Applications

The International Telecommunication Union (ITU) divided the world into three regions to manage the global allocation of the radio frequency spectrum as illustrated in the map in Figure 2.6. South Africa falls under ITU Region 1 and therefore allocates its frequency according to specifications for ITU Region 1. Although this is the case, each country has a telecommunication regulation organisation which regulates the use of the radio frequency (RF) spectrum in that particular country. In South Africa it is regulated by the Independent Communications Authority of South Africa (ICASA) and in North America the most prominent organisation is the Federal Communications Commission (FCC). The use of radio frequencies for broadcasting is regulated and allocated to users by these organisations.

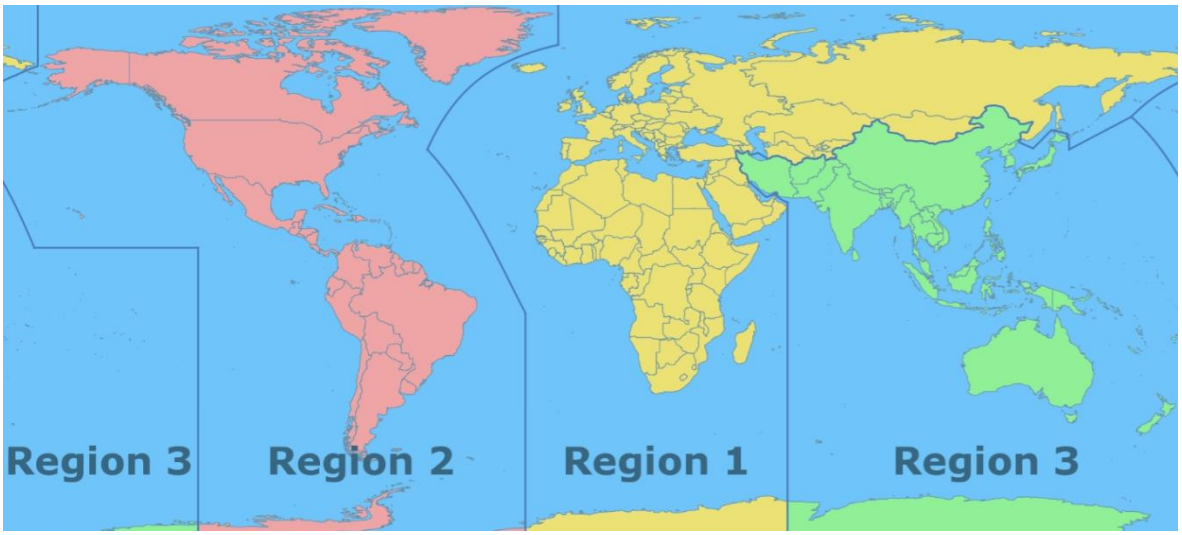

Figure 2. 6: ITU Region Map for Frequency Allocations [50]

According to [67], the National Rural Telecommunications Cooperative (NRTC) in the United States of America (USA) purchased a licence to use the 220MHz frequency for use in electricity SCADA systems. It is an example of the VHF frequency being exploited successfully for SCADA systems. Also, the Scheneider - Electric group has recently released a Trio QR 150 high-speed digital data radio for SCADA applications. This digital radio operates at the VHF frequency range of 135 - 175MHz [68]. Therefore, the VHF frequency band is currently being widely used for SCADA purposes, however, thus far there is no evidence of it used in the low VHF frequency band with the MIMO technology to mitigate propagation challenges in irregular terrain environments especially in the South African context. According to a report in [48], the MIMO technology in South Africa has only been used for Long Term Evolution (LTE) networks by the cellular phone industry to achieve increased throughput and improved the network capacity.

2.8 The MIMO and OSTBC Technologies Applied in Wireless Communication

For simplicity in explanation, the Alamouti code is used in this section.

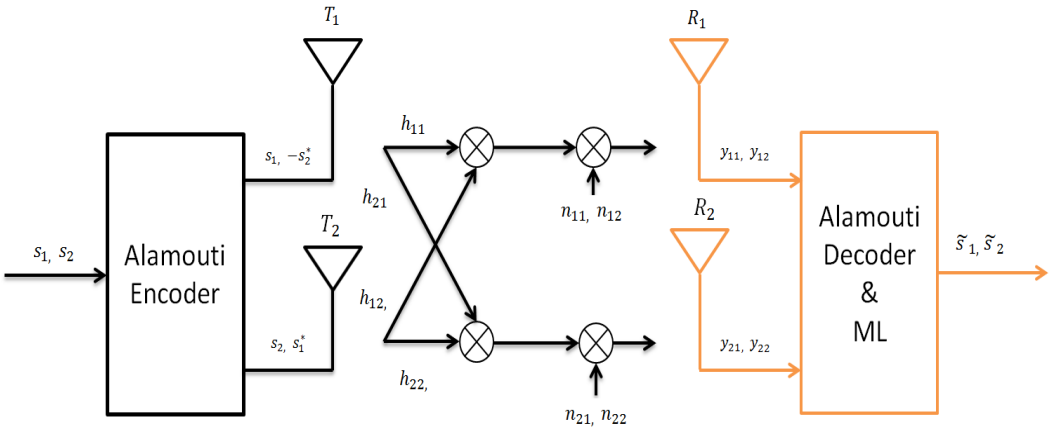

Figure 2. 7: MIMO 2x2 System with Alamouti Coding [63]

Figure 2.7 shows an OSTBC 2x2 MIMO system diagram, from which the following brief system operation is taken. For the two receive antennas, the received symbols are the following:
In the first time slot ts_1, the received signal is represented by the following equation:

$$\begin{bmatrix} y_1^1 \\ y_2^1 \end{bmatrix} = \begin{bmatrix} h_{11} & h_{12} \\ h_{21} & h_{22} \end{bmatrix} \begin{bmatrix} s_1 \\ s_2 \end{bmatrix} + \begin{bmatrix} n_1^1 \\ n_2^1 \end{bmatrix} \quad (2.10)$$

The following equation will apply for the received signal in the second time slot ts_2:

$$\begin{bmatrix} y_1^2 \\ y_2^2 \end{bmatrix} = \begin{bmatrix} h_{11} & h_{12} \\ h_{21} & h_{22} \end{bmatrix} \begin{bmatrix} -s_2^* \\ s_1^* \end{bmatrix} + \begin{bmatrix} n_1^2 \\ n_2^2 \end{bmatrix} \quad (2.11)$$

Where:

$\begin{bmatrix} y_1^1 \\ y_2^1 \end{bmatrix}$ = Time slot one received signal, on antenna 1 and 2,

$\begin{bmatrix} y_1^2 \\ y_2^2 \end{bmatrix}$ = Time slot two received signal, on antenna 1 and 2,

h_{ij} = Rayleigh channel from i^{th} receive antenna to j^{th} transmit antenna,

$s_1 \; and \; s_2$ = transmitted symbols,

$\begin{bmatrix} n_1^1 \\ n_2^1 \end{bmatrix}$ = AGWN at time slot one, on receive antenna 1 and 2,

$\begin{bmatrix} n_1^2 \\ n_2^2 \end{bmatrix}$ = AGWN at time slot two, on receive antenna 1 and 2,

At the combiner, time slot one and two equations will be combined thus:

$$\begin{bmatrix} y_1^1 \\ y_2^1 \\ y_1^{2*} \\ y_2^{2*} \end{bmatrix} = \begin{bmatrix} h_{11} & h_{12} \\ h_{21} & h_{22} \\ h_{12*} & h_{11*} \\ h_{22*} & h_{21*} \end{bmatrix} \begin{bmatrix} s_1 \\ s_2 \end{bmatrix} + \begin{bmatrix} n_1^1 \\ n_2^1 \\ n_1^{2*} \\ n_2^{2*} \end{bmatrix} \quad (2.12)$$

At the receiver the Maximum Likelihood (ML) decoder recovers reliable estimates of the original data sent. Despite the severity of the propagation channel, the transmitted symbols are recovered through other propagation paths. The recovered data is expressed by the following matrix:

$$\begin{bmatrix} \tilde{s}_1 \\ \tilde{s}_2 \end{bmatrix} = \begin{bmatrix} h_{11}^* & h_{21}^* & h_{12} & h_{22} \\ h_{12}^* & h_{22}^* & -h_{11} & -h_{21} \end{bmatrix} \begin{bmatrix} y_{11} \\ y_{21} \\ y_{12}^* \\ y_{22}^* \end{bmatrix} \quad (2.13)$$

2.9 Conclusion

This chapter provided an overview of various factors affecting wireless communication over different propagation environments. Some methods to mitigate these factors, especially in irregular terrain environments, were discussed. It also presented recent developmental studies on technologies such as MIMO and OSTBC to efficiently improve wireless communication challenges in irregular terrain. Technologies which have captured the attention of researchers in wireless communication and certainly of great interest in this research were:

- Multiple-In Multiple Out (MIMO)
- Orthogonal Space Time Block Codes (OSTBC)

Multiple-In Multiple-Out (MIMO): MIMO is a technology which uses multiple antenna arrays at both the transmitter and receiver. The multiple antennas cause the MIMO system to achieve beamforming, full diversity, less interference, spatial multiplexing and high data rates. Orthogonal Space Time Block Codes (OSTBC): OSTBC is a method of coding data that uses two or more transmit antennas. It enhances the MIMO system by providing greater reliability, increased capacity and less bit errors.

CHAPTER 3: MODELLING OF THE OSTBC MIMO TRANSCEIVER SYSTEM IN A RAYLEIGH FADING PROPAGATION CHANNEL

3.1 Introduction

In this chapter, the mathematical modelling of the operation of the Orthogonal Space-Time Block Code, Multiple In - Multiple Out (OSTBC MIMO) transceiver system in a Rayleigh fading propagation channel is discussed. The model is developed using Matlab/Simulink software.

The OSTBC MIMO transceiver model consists of a Random Binary Generator (RBG) which generates an unpredictable binary sequence which is used to model the radio signal data. The RBG is then coupled to a Quadrature Phase Shift Keying (QPSK) modulator, which modulates the binary data from the RBG into data symbols which are twice the bit duration. The QPSK modulator has been selected over other low order modulation schemes such as Binary Phase Shift Keying (BPSK) for this reason, that is, its ability to produce increased data rates and more efficient results than BPSK, M-PSK or QAM [69]. The modulated data symbols are then presented to the input of an OSTBC Encoder which maps the data symbols for multiple transmitting antennas using the OSTBC code. The encoded data is then transmitted over the channel. The requirement for OSTBC Encoder is the use of multiple antennas, which yields high capacity and fewer error rates. Another attractive trait of the OSTBC Encoder which led to its election for this research is its low complexity receiver design and high diversity gains [70]. The Rayleigh fading and AWGN stages are used to model the fading, non-line of sight, noisy propagation channel. Rayleigh fading model is chosen over other models such as Rician fading model because this study investigates a non-line of sight environment, which the Rayleigh model is used for. The Rician model on the other hand models a multi-path channel with at least one strong line of sight path [81]. The OSTBC Decoder combines the received signals from the receiving antennas and the Channel State Information (CSI) to be able to recover the data of the symbols. The QPSK demodulator is the final recovery stage of the model. It demodulates the received data symbols into the originally sent data bits. The OFDM modulation scheme which is usually recommended for use with the MIMO technology because of its great data rate capability was considered for this model. However, OFDM uses multiple modulation schemes in one system, which contributes to complexity and

cost. On the other hand, OSTBC with MIMO yields great data rates also through diversity. It is less complex and uses only one modulation scheme. Also, the use of OSTBC provides channel coding which helps in improving the error performance, so as to enhance efficiency of data transmission over noisy channels [69]. VHF band was chosen over the HF band because it has a bigger working bandwidth and less noisy.

The selection of the low VHF frequency band (49-108 MHz) to use with the OSTBC MIMO system as illustrated in Section 4.3 is due to findings presented in the literature in Chapter 2. The literature revealed that the general use of lower frequencies in irregular terrain environments tends to produce diffraction [11 and 22]. Diffraction causes radio signals to move around or over obstructions such as high mountains without hindrance. However, the drawback of employing low frequencies is that they have low data rates and a small working bandwidth [23].
Although this is the case, [40] discovered that better bandwidth utility and high data rates at Very Low Frequencies can be achieved by using a higher-order modulation scheme. Due to this revelation, the VHF frequency band was the choice band to exploit as it is neither too low nor too high. A high order modulation scheme has been used in this model. In this case it is QPSK modulation. Employing this modulation scheme along with a high capacity, full diversity OSTBC MIMO system, the VHF band would be a suitable band to use for the SCADA system in irregular terrain for Eskom.

As has been highlighted in the literature in Section 2.7, the VHF frequency band is currently being widely used for SCADA purposes, however, it has not been used in the low band VHF frequency with the MIMO technology to mitigate propagation challenges in irregular terrain environments especially in the South African context. This research is exploiting the low band VHF frequency of 70MHz to obtain the anticipated results. The only drawbacks for Eskom utilising this model practically is that Eskom is currently not licenced to operate in the said frequency band. Therefore, ICASA would have to be consulted about the radio communication services permitted in this band. Furthermore, the market currently does not have OSTBC MIMO data radios operating at 70MHz. However, there are prospects of having a MIMO radio operating at lower VHF frequencies.
Therefore, the proposed model was developed in Matlab/Simulink and presented with the aim to transmit data employing the OSTBC MIMO technology in a multi-path fading, noisy channel,

typical that of an irregular terrain environment, and recover it successfully at the receiver. Bit Error Rate (BER) graphs and propagation predictions were used to analyse the model.

Section 3.2-3.8 discusses the relevant components of the system. Section 3.10 presents the conclusion of the chapter.

3.2 Random Binary Generator

All relevant factors with regards to the operation of the proposed OSTBC MIMO transceiver system need to be taken into account if a mathematical model is to be developed. Figure 3.1, shows a random binary generator block diagram, whose function is to generate an unpredictable binary sequence. In this model it is used to simulate data to be sent over the medium.

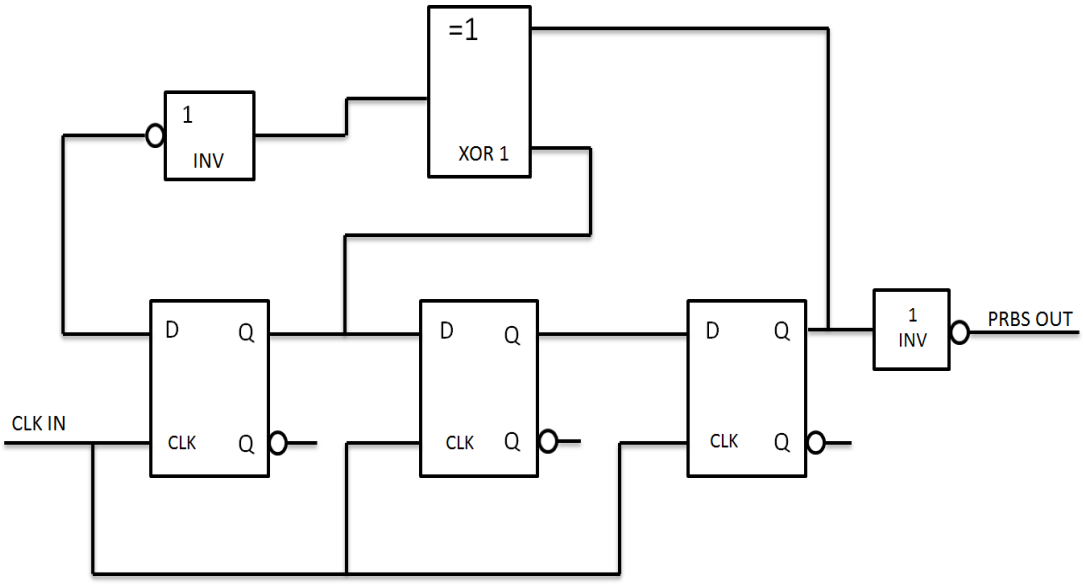

Figure 3. 1: Random Binary Generator Block Diagram

Pseudorandom binary sequences (PRBS) bit stream can be generated using linear-feedback shift registers (LFSR) as seen in Figure 3.1 [71]. For simplicity in explanation, Figure 3.1 illustrates an example of a simple 3-bit LFSR where the first bit is filled with the exclusive-or (XOR) of two other bits in the shift register [72].

The shift register is filled up by the Clock (CLK IN) input with a seed pattern of pulses to initiate the operation. At each time step the bits contained in selected positions in the shift register are combined using an exclusive-or (XOR) gate and the result is fed back into the register's input bit. The register is shifted by one bit, and the result of the feedback is entered into the shift register due to the shifting bits, thus occupying the location that is vacant as a consequence of the shift. The pattern repeats endlessly. The length of the pattern is 7 different bit combinations. This is the maximum possible. There are at most 8 different bit combinations in a 3-bit register (2 to the power 3). It is this feedback that causes the register to loop through and give an output of repetitive sequences of pseudo-random (PRBS OUT) bits [73]. A binary sequence is illustrated in equation (3.1):

$$a_0, \dots a_{N-1} \qquad of\ N\ bits \tag{3.1}$$

$$a_j \in \{0, 1\} \text{ for } j = 0,1, \dots, N-1. \tag{3.2}$$

Therefore, a binary sequence (BS) will consist of the follow [74],

Where:

$m = \sum a_j =$ (ones).

$N - m =$ (zeros).

A pseudorandom binary sequence is a (BS) with an autocorrelation function expressed by the following equation [75]:

$$C(v) = \sum_{j=0}^{N-1} a_j a_{j+v} \tag{3.3}$$

It has two values:

$$C(v) = \begin{cases} m, if\ v \equiv 0\ (mod\ N) \\ mc,\ otherwise \end{cases} \tag{3.4}$$

Where:

$c = \frac{m-1}{N-1}$ = duty cycle.

It is pseudorandom because a_j is independent of values of other elements, similar to real random sequences. The output (PRBS OUT) of the random binary generator is fed to the input of the QPSK Modulator.

3.3 Quadrature Phase Shift Keying (QPSK) Modulator

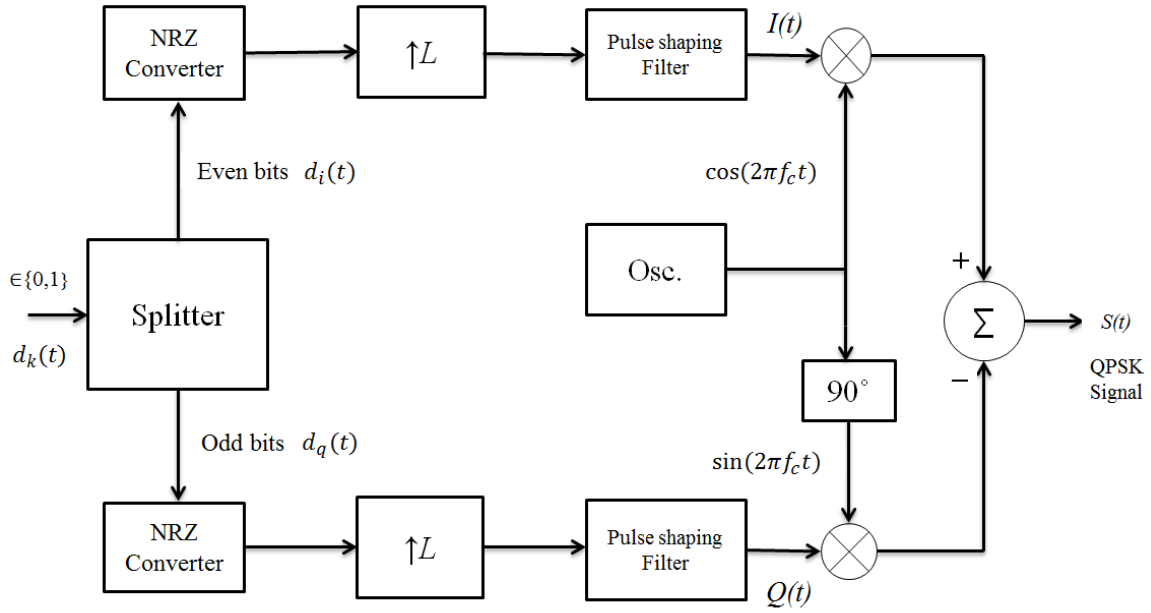

Figure 3. 2: QPSK Modulator Block Diagram

The binary output data from the random binary generator is then fed to the modulation stage input $d_k(t)$. Figure 3.2, is an illustration of the QPSK modulator stage. In this stage, a splitter divides the binary data stream:

$$d_k(t) = d0, d1, d2, d3, \ldots \text{ into two data streams,} \quad (3.5)$$

$$d_q(t) = d1, d3, d5, \ldots \text{ and} \quad (3.6)$$

$$d_i(t) = d0, d2, d4, \ldots \quad (3.7)$$

Where:

$d_k(t)$ = generated binary stream.

$d_q(t)$ = odd bits (quadrature stream).

$d_i(t)$ = even bits (in-phase stream).

Each of these bits are converted to Non-Return-to-Zero (NRZ) pattern in a parallel manner. The QPSK modulation technique sends two bits of digital data at time, therefore this means after oversampling and pulse shaping, the symbol duration of both $d_q(t)$ and $d_i(t)$ streams are twice the bit duration ($T_{sym} = 2T_b$), thus increasing the data rate as seen in Figure 3.3 [76].

Where:

T_{sym} = symbol duration.

T_b = bit duration.

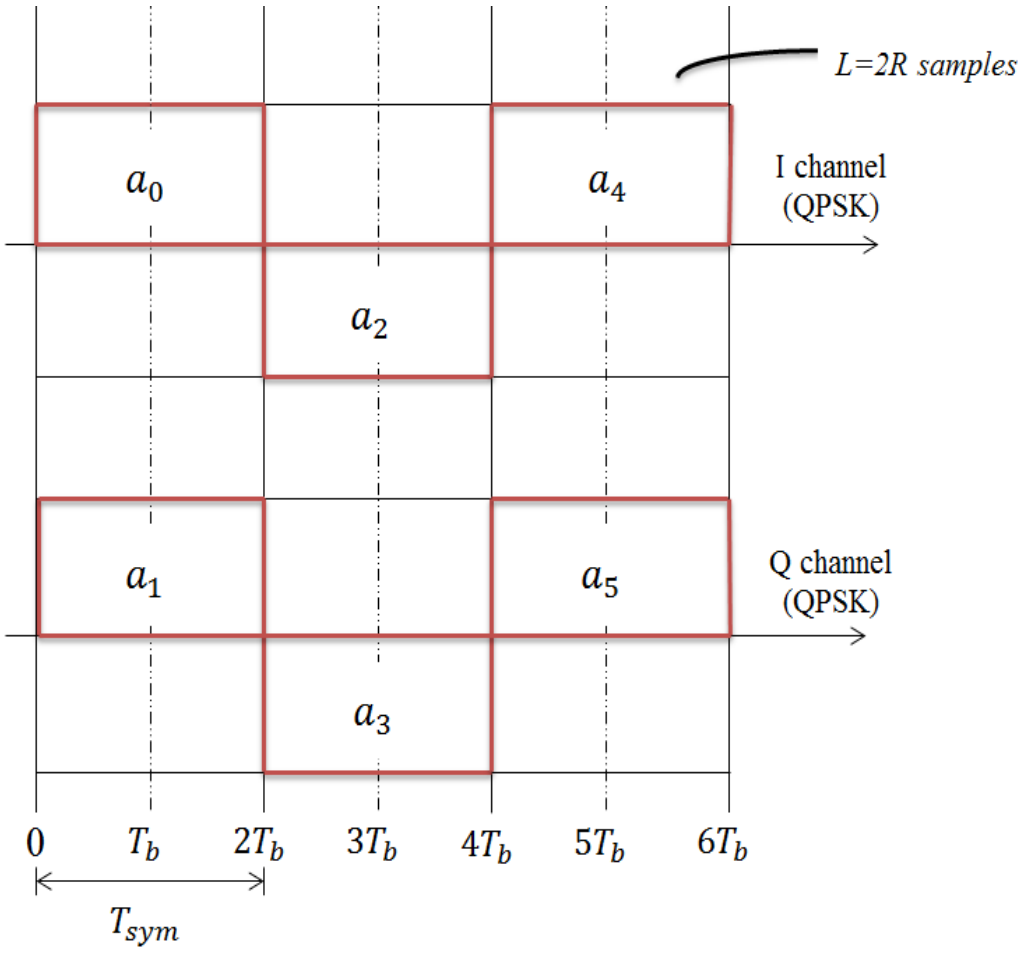

Figure 3. 3: Timing Diagram for QPSK Modulation.

The oversampling rate is selected as:

$$L = \frac{2f_s}{f_c} \tag{3.8}$$

Where:

f_s = Sampling frequency.

f_c = Carrier frequency.

The balanced modulators amplitude modulate each of the in-phase $I(t)$ and quadrature $Q(t)$ signals, by multiplying them with the carrier, known as the cosine and sine functions respectively. The quadrature $Q(t)$ signal, however, is phase shifted by 90° before modulation. The following are the modulated in-phase $I(t)$ and quadrature $Q(t)$ signals [77]:

$$I(t)\ \cos(2\pi f_c t) \tag{3.9}$$

$$-Q(t)\ \sin(2\pi f_c t) \tag{3.10}$$

Where:

$I(t)$ = baseband in-phase signal.

$Q(t)$ = baseband quadrature signal.

f_c = carrier frequency.

t = time base for carrier modulated signal.

The quadrature phase shifter will produce four possible carrier phase shift states, derived from the following signal phase equation:

$$\theta_n = (2_n - 1) \times \frac{\pi}{4} \tag{3.11}$$

Where:

θ_n = signal phase.

n = 1,2,3,4.

Therefore, the four possible signal phases are:

$\frac{\pi}{4},\ 3\frac{\pi}{4},\ 5\frac{\pi}{4}\ and\ 7\frac{\pi}{4}$ radians.

The Summing Amplifier produces the required QPSK modulated signal $S(t)$, by adding the in-phase $I(t)$ and quadrature $Q(t)$ signals at different phases thus producing the following equation [78]:

$$S(t) = \frac{1}{\sqrt{2}} I(t)\ \cos[2\pi f_c t + \theta_n] - \frac{1}{\sqrt{2}} Q(t)\ \sin(2\pi f_c t + \theta_n) \tag{3.12}$$

The above equation can also be written using trigonometric identities as:

$$S(t) = \cos[2\pi f_c t + \theta_n] \tag{3.13}$$

3.4 Orthogonal Space Time Block Code (OSTBC) Encoder

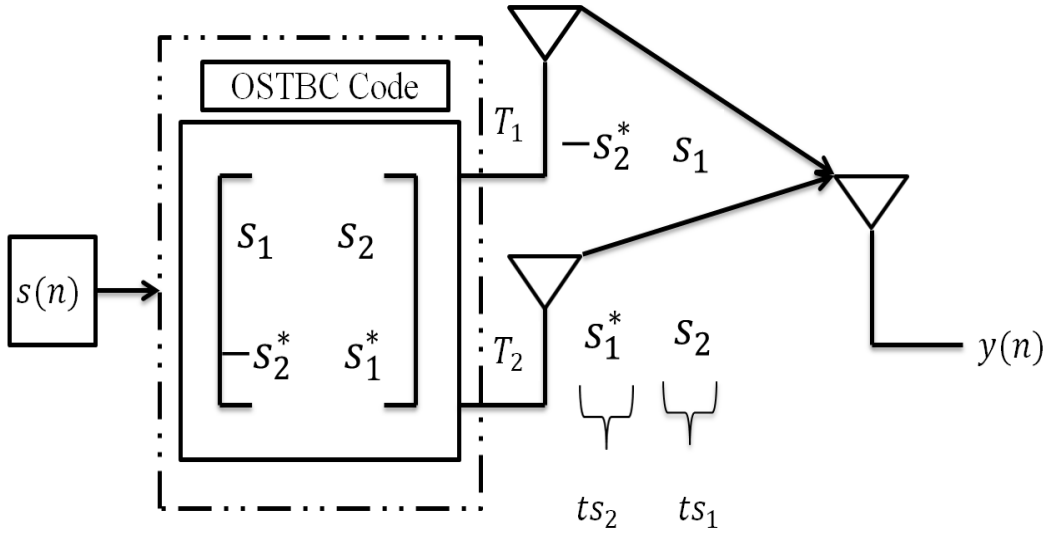

Figure 3. 4: Orthogonal Space Time Block Code (OSTBC) Encoder Diagram

In MIMO systems, the capacity of the channel can be increased by using spatial multiplexing. However, to increase the reliability of the channel, space time coding (STC) is used [52].

Space Time Block Code (STBC) is a technique derived from Alamouti's scheme [62], to send data streams via a MIMO system over two transmit antennas T_1 and T_2.

Orthogonal Space Time Block Code (OSTBC) is fundamentally the Alamouti code with a complex orthogonal generalised code for three or four transmit antennas [79]. There is no difference in encoding and decoding between STBC and OSTBC. The data to be transmitted is converted to a matrix S_n whose columns represent the number of transmit antennas (T_1 and T_2) and the rows represent the number of time slots ts_1 and ts_2 necessary to transmit data.

Figure 3.4 shows an OSTBC encoder diagram where orthogonal codes (S_1) and (S_2) are transmitted over antennas (T_1) and (T_2) in the first time slot (ts_1), while the other part of the codes ($-S_2^*$ and S_1^*) are transmitted in the second time slot (ts_2). Since the STBC and OSTBC are the same, except for the complexity which comes with the use of multiple antennas in OSTBC, the Alamouti code will be discussed in this section, for purposes of simplicity of explanation. Therefore, the output of the QPSK Modulator which contains data symbols is presented to the

input of the OSTBC Encoder stage which encodes the data symbols by using OSTBC scheme [80]. The output of the OSTBC module is a variable of ($N_s \times N_t$) size matrix.

Where:

N_t = represents the number of transmitting antennas and the number of columns in the matrix.

N_s = represents the number times slots and the number of rows in the matrix.

The function of the OSTBC Encoder is to encode an algorithm for defined number of transmit antennas. It entails transmitting the data signal (S_n) over two different time slots over two different antennas [62]. The data signal (S_n) can be de-multiplexed and transmitted over two antennas as subsets (S_1) and (S_2) of the encoding matrix (S_n) thus:

$$S_1 = \frac{1}{\sqrt{2}} S(n) \tag{3.14}$$

$$S_2 = \frac{1}{\sqrt{2}} S(n) \tag{3.15}$$

Where:

n = The prevailing discrete signal block.

The transmitted data signal equations(S_1, S_2) can also be expressed as:

$$S_1, S_2 = \in C^{\left(\frac{N}{N_T \times 1}\right)} \; \forall \, N_T = 2 \tag{3.16}$$

Where:

N_T = The maximum number of transmit antennas.

$\in C^{(.)}$ = The transmitted data signal energy complex matrix.

The encoding matrix of the above equation can be expressed as:

$$S_n = \begin{bmatrix} S_1 & S_2 \\ -S_2^* & S_1^* \end{bmatrix} \quad (3.17)$$

Suppose that the signal energy on each antenna is 1, therefore the matrix(S_n) will be an orthogonal matrix. Because there are N_T transmitting antennas, the codes (and their respective conjugates) can be expressed as:

$$S_1, S_2 = \in C^{\left(\frac{N}{N_T}\right)\times N_R} \quad (3.18)$$

Where:

N_R = is the number of receive antennas.

Let us suppose that N_R is 1. Equation (3.18) above allows that the system operates with full transmission rate and diversity. There are two time slots and two antennas.

In a MIMO transceiver system, if the number of time slots (T)and the number of antennas are equal to unity, that system will operate with full transmission rate.

3.5 Multipath Rayleigh Fading Channel

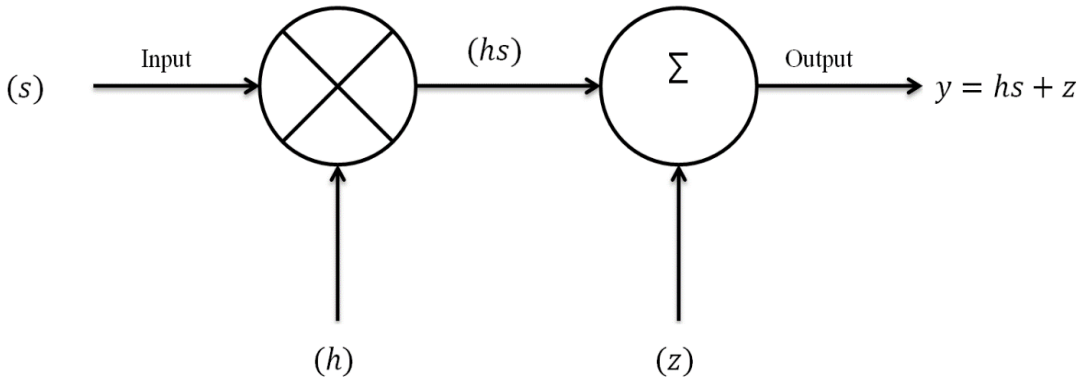

Figure 3. 5: Multipath Rayleigh Fading Channel Diagram

The transmitted signals from the MIMO antennas in the Orthogonal Space Time Block Code (OSTBC) stage are propagated through the medium taking multiple paths to the receiver. Figure 3.5 illustrates the fading channel. The harsh propagation environment of the MIMO transceiver used in this research is modelled by both the Rayleigh fading channel and the AWGN expressed in the following equation:

$$y = hs + z \tag{3.19}$$

Where:

y = The output signal.

h = The frequency flat fading channel.

s = The signal being transmitted.

z = The noise term of the Additive White Gaussian Noise (AWGN).

The Multipath Rayleigh Fading Channel models a baseband multipath Rayleigh fading propagation channel typical that of a non-line of sight, irregular, mountainous terrain.

Because a multi-path channel reflects, scatters and refracts signals, a transmitted signal takes many different paths to the receiver, which paths may vary in lengths and associated time delays. (h) which is the frequency flat fading channel component in the transceiver system can be expressed from the multi-path Rayleigh model as:

$$h_{i=} \sum_{k=0}^{N-1} u_k e^{j\theta_k}, \forall i = 1,2,\dots,N_T \tag{3.20}$$

Where:

u = The gain corresponding to k^{th} path.

N = The maximum number of the resolvable multipath.

θ = The phase.

N_T = The maximum number of transmit antennas.

The channel h, in Equation (3.19) is a matrix containing:

$$h = \quad [h_1 \quad h_2]^T \tag{3.21}$$

Where:

$[\,.\,]^T$ = The Hermitian transpose.

Because the model is a frequency flat fading channel, the amplitude (u_k) is uniform for all N paths of the channel [81]. Rayleigh fading has a level crossing rate, which measures how quickly fading takes place in a specific channel. It informs us of how often the fading crosses a certain threshold in the transmit direction. It is measured using the following equation [82]:

$$LRC = \sqrt{2\pi} f_d \rho e^{-p2} \tag{3.22}$$

Where:

$f_d =$ Maximum Doppler shift.

ρ = Threshold level normalised to the root-mean-square (RMS) signal level, represented by the following equation:

$$\rho = \frac{R_{threshold}}{R_{rms}} \tag{3.23}$$

The average fade duration (AFD), measures how long the signal stays below the threshold (ρ). AFD for Rayleigh fading is [82]:

$$AFD = \frac{e^{p2}-1}{\rho f_d \sqrt{2\pi}} \tag{3.24}$$

The average fade duration (AFD) and the level crossing rate (LCR), both help determine how sever the fading could be in a channel is over time.

3.6 Additive White Gaussian Noise (AWGN)

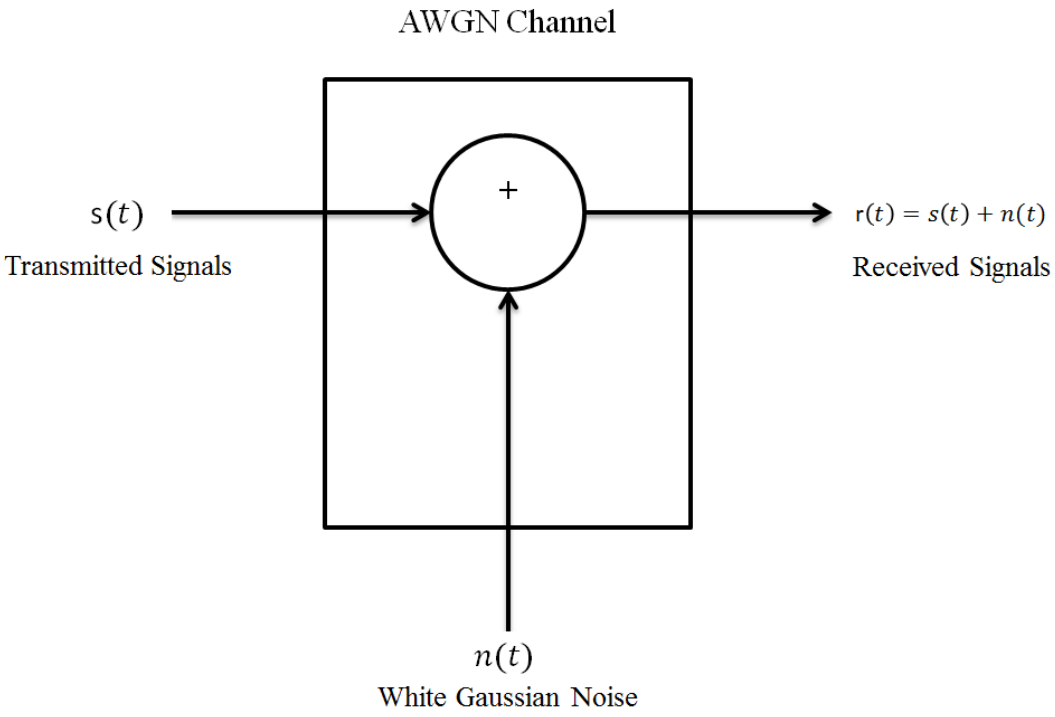

Figure 3. 6: AWGN Channel Diagram

Random noise in the propagation channel can cause transmitted data to be corrupted such that the receiver interprets it differently in the modulation scheme alphabet. The AWGN channel shown in Figure 3.6, models symbol errors resulting from a noisy propagation channel. This noise channel model is typical to that of the irregular terrain environment in the Northern Cape. The symbol errors generated by the model cause bit errors at the output, which is the input of the receiver. Additive White Gaussian Noise (AWGN) is a wide frequency range of natural noises that are added to a radio communication channel which is independent of the actual transmitted signal. Its power spectral density is flat and its noise samples have a Gaussian distribution [83]. AWGN channel is represented by the following equation:

$$r(t) = s(t) + n(t) \tag{3.25}$$

Where:

$r(t)$ = Receive signal, at discrete time intervals (t).

$s(t)$ = Transmit signal.

$n(t)$ = Natural independent random noise.

The receive signal $r(t)$, which is the sum of the transmit signal $s(t)$ and the random noise $n(t)$ in the medium is then be presented to the OSTBC Decoder which is the receive stage.

3.7 Orthogonal Space-Time Block Codes (OSTBC) Decoder

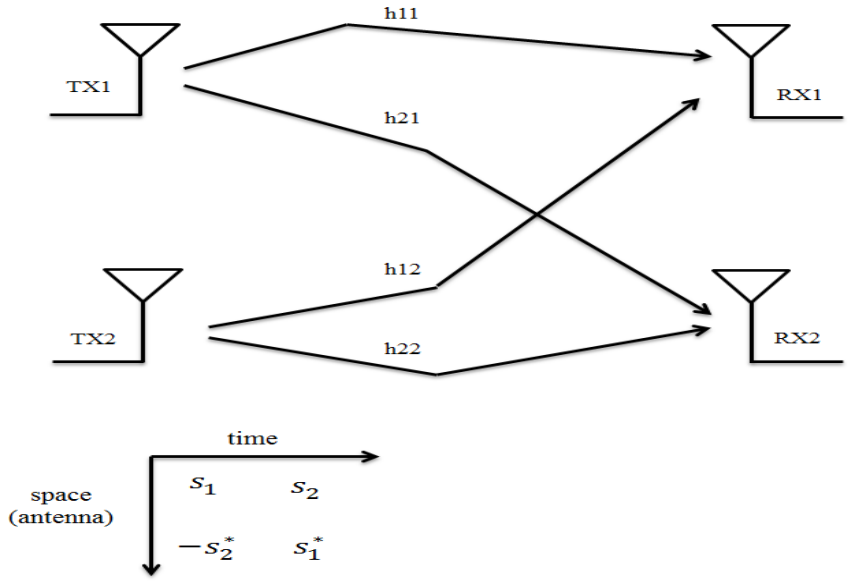

Figure 3. 7: Orthogonal Space-Time Block Codes (OSTBC) Decoder Diagram

The Orthogonal Space-Time Block Codes (OSTBC) Decoder stage as seen in Figure 3.7 combines the received signals from the receive antennas and the Channel State Information (CSI) in order to recover the information of the symbols encoded by the OSTBC encoder. For discussion on the received signal by the OSTBC decoder, the channel and noise model will also be discussed. In the first time slot, the received signal is represented by the following equation:

$$\begin{bmatrix} y_1^1 \\ y_2^1 \end{bmatrix} = \begin{bmatrix} h_{11} & h_{12} \\ h_{21} & h_{22} \end{bmatrix} \begin{bmatrix} s_1 \\ s_2 \end{bmatrix} + \begin{bmatrix} n_1^1 \\ n_2^1 \end{bmatrix} \quad (3.26)$$

If the channel remains unchanged, the following equation will apply for the received signal in the second time slot:

$$\begin{bmatrix} y_1^2 \\ y_2^2 \end{bmatrix} = \begin{bmatrix} h_{11} & h_{12} \\ h_{21} & h_{22} \end{bmatrix} \begin{bmatrix} -s_2^* \\ s_1^* \end{bmatrix} + \begin{bmatrix} n_1^2 \\ n_2^2 \end{bmatrix} \quad (3.27)$$

Where:

$\begin{bmatrix} y_1^1 \\ y_2^1 \end{bmatrix}$ = Time slot one received signal, on antenna 1 and 2,

$\begin{bmatrix} y_1^2 \\ y_2^2 \end{bmatrix}$ = Time slot two received signal, on antenna 1 and 2,

h_{ij} = Rayleigh channel from i^{th} receive antenna to j^{th} transmit antenna,

$s_1 \; and \; s_2$ = transmitted symbols,

$\begin{bmatrix} n_1^1 \\ n_2^1 \end{bmatrix}$ = AGWN at time slot one, on receive antenna 1 and 2,

$\begin{bmatrix} n_1^2 \\ n_2^2 \end{bmatrix}$ = AGWN at time slot two, on receive antenna 1 and 2,

At the decoder, time slot one and two equations are combined thus [75]:

$$\begin{bmatrix} y_1^1 \\ y_2^1 \\ y_1^{2*} \\ y_2^{2*} \end{bmatrix} = \begin{bmatrix} h_{11} & h_{12} \\ h_{21} & h_{22} \\ h_{12*} & h_{11*} \\ h_{22*} & h_{21*} \end{bmatrix} \begin{bmatrix} s_1 \\ s_2 \end{bmatrix} + \begin{bmatrix} n_1^1 \\ n_2^1 \\ n_1^{2*} \\ n_2^{2*} \end{bmatrix} \quad (3.28)$$

$$\text{Let } H = \begin{bmatrix} h_{11} & h_{12} \\ h_{21} & h_{22} \\ h_{12*} & h_{11*} \\ h_{22*} & h_{21*} \end{bmatrix} \quad (3.29)$$

Therefore, to find $\begin{bmatrix} s_1 \\ s_2 \end{bmatrix}$, the inverse of H needs to be known. For a general matrix the pseudo inverse equation is:

$$H^{+} = (H^{H}H)^{-1}H^{H} \tag{3.30}$$

Therefore, the recovered original transmitted symbol will be:

$$\begin{bmatrix} s_1 \\ s_{2*} \end{bmatrix} = (H^{H}H)^{-1}H^{H} \begin{bmatrix} y_1^1 \\ y_2^1 \\ y_1^{2*} \\ y_2^{2*} \end{bmatrix} \tag{3.31}$$

We observe that the use of OSTBC using 2 receive antennas over two symbols results in a diversity order of 4. In general, with N receiving antennas, the diversity order for 2 transmitting antennas in Alamouti's STBC is $2N$. This theory increases capacity and the recovery rate at the receiver [85].

3.8 Quadrature Phase Shift Keying (QPSK) Demodulator

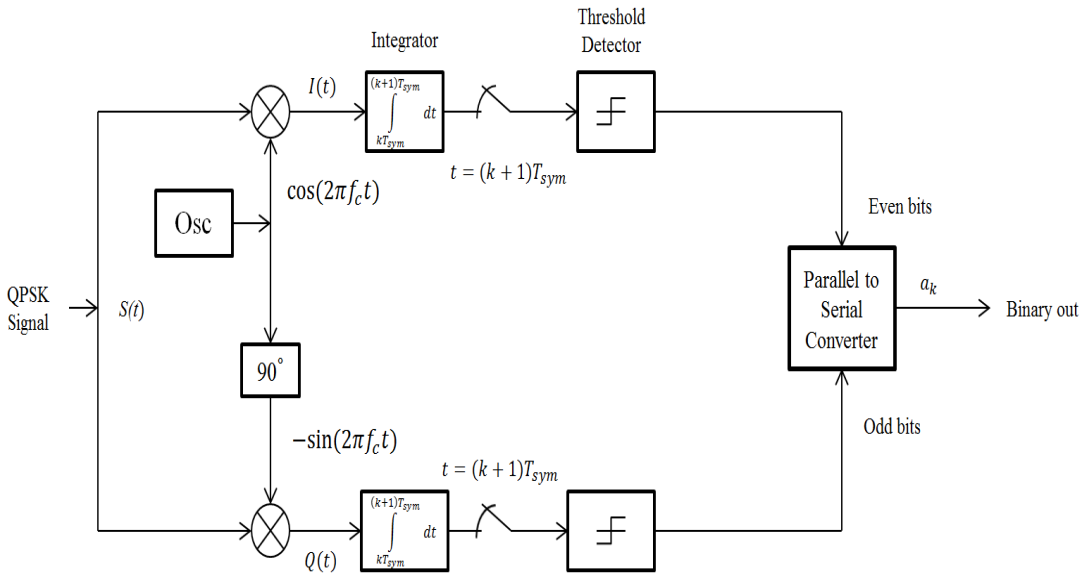

Figure 3. 8: QPSK Demodulator Block Diagram

From the output of the OSTBC Decoder, the data is fed into the QPSK Demodulator. The QPSK Demodulator illustrated in Figure 3.8 makes use of a control system called the Phase Lock Loop (PLL) to determine the carrier frequency and the phase as these must be known to the receiver. The PLL simply locks the incoming carrier frequency and traces the changes in frequency and phase and generate an output related to the changes. In the demodulator, the incoming data signal is multiplied by the reference frequency generators $\cos(2\pi f_c t)$ and $-\sin(2\pi f_c t)$ on the in-phase and quadrature arms respectively to recover the $I(t)$ and $Q(t)$ signals [86].

Where:

f_c = carrier frequency.

t = time base for carrier modulated signal.

The multiplied outputs $I(t)$ and $Q(t)$ on each arm are then applied to an integrator, which integrates the output over one-bit period. The decision block is a threshold detector which decides on whether a 0 or a 1 is detected based on a reference threshold value. The even and odd bits on each arm are passed to the parallel to serial converter where they are recovered to form the original generated data [87].

Where:

$I(t)$ = in-phase signal.

$Q(t)$ = quadrature signal.

$$\text{Let} \quad (2\pi f_c t) = \omega(t) \tag{3.32}$$

Therefore, by multiplying $\sin \omega t$ by a phase shifted signal$(\sin \omega t + \theta)$, this gives a demodulated signal which is double the input signal, with a DC offset which changes based on the phase shiftθ [78]. To test this theory $(\sin \omega t)$ is multiplied by a shifted sine wave$(\sin \omega t + \theta)$:

$$(\sin \omega t) \times (\sin \omega t + \theta) = \frac{e^{j\omega t} - e^{-j\omega t}}{2j} \times \frac{e^{j(\omega t+\theta)} - e^{-j(\omega t+\theta)}}{2j} \tag{3.33}$$

$$= \frac{e^{j(2\omega t+\theta)} - e^{j(\omega t-\omega t-\theta)} - e^{j(\omega t+\theta-\omega t)} + e^{-j(2\omega t+\theta)}}{-4} \tag{3.34}$$

$$= \frac{\cos(2\omega t+\theta)}{-2} - \frac{e^{j\theta}+e^{-j\theta}}{-4} \tag{3.35}$$

$$= \frac{\cos(2\omega t+\theta)}{-2} + \frac{\cos\theta}{2} \tag{3.36}$$

$$= \frac{\cos\theta}{2} - \frac{\cos(2\omega t+\theta)}{2} \tag{3.37}$$

In the equation above it is shown that the phase shift on a carrier can be demodulated into a changing output voltage by multiplying the carrier and the local oscillator frequency and filtering out the high frequency portion. To decode phase shifts in all quadrants, the input signal needs to be multiplied by both sine and cosine signals, the high frequency filtered out and the data recovered [86]. Below this is further proven:

$$(\cos\omega t) \times (\sin\omega t + \theta) = \frac{e^{j\omega t}+e^{-j\omega t}}{2} \times \frac{e^{j(\omega t+\theta)} - e^{-j(\omega t+\theta)}}{2j} \tag{3.38}$$

$$= \frac{e^{j(2\omega t+\theta)} - e^{j(-\theta)} + e^{j(\theta)} - e^{-j(2\omega t+\theta)}}{-4j} \tag{3.39}$$

$$= \frac{\sin(2\omega t+\theta)}{2} + \frac{e^{j\theta}-e^{-j\theta}}{4j} \tag{3.40}$$

$$= \frac{\sin(2\omega t+\theta)}{2} + \frac{\sin\theta}{2} \tag{3.41}$$

3.9 Proposed OSTBC MIMO Model

The proposed OSTBC-MIMO transceiver model over a Rayleigh fading channel is shown in Figure 3.9. The model is simulated using MATLAB/Simulink software. The following are the different component blocks making up the system:

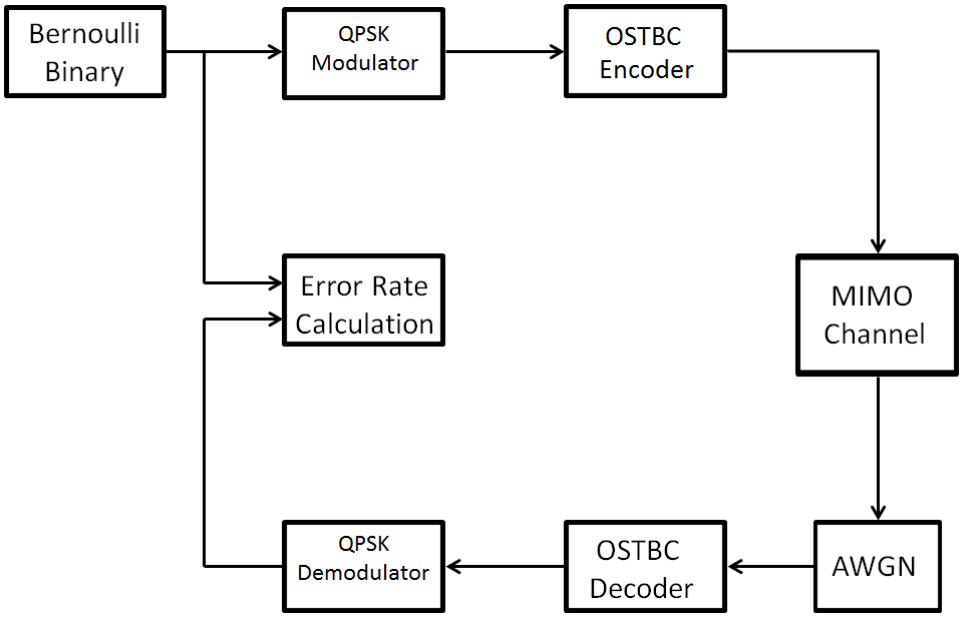

Figure 3. 9 Proposed OSTBC MIMO Model

- Random Binary Generator

The random binary generator generates a binary sequence that is unpredictable. These random bits are used to simulate the information to be transmitted over the medium.

- Quadrature Phase Shift Keying (QPSK) Modulator

The binary data from the random binary generator is modulated using a QPSK modulation scheme. In this block, a splitter divides the binary data stream into two data streams, $d_q(t)$ and $d_i(t)$. The symbol duration for both $d_q(t)$ and $d_i(t)$ streams are twice the bit duration ($T_{sym} = 2T_b$), thus increasing the data rate [69]. At the output the two modulated data signals $I(t)\cos(2\pi f_c t)$ and $Q(t)\sin(2\pi f_c t)$, are added to form a QPSK modulated signal $S(t)$.

- Orthogonal Space-Time Block Code (OSTBC) Encoder

The output of the QPSK Modulator which contains data symbols is fed into the input of the OSTBC Encoder which encodes the data symbols by either using the Alamouti code [62] for two transmit antennas or a complex orthogonal code for three or four transmit antennas [80]. In this model, a 4X4 MIMO system with four antennas is implemented [88]. The block maps the input symbols block-wise and concatenates the output code matrices in the time domain.

- Multiple-In Multiple-Out (MIMO) Rayleigh Fading Channel

The MIMO Rayleigh Fading Channel block models a baseband multipath fading channel typical that of a non-line of sight, irregular, mountainous terrain. The block is configured as a 4x4 MIMO channel with transmitting and receiving antenna selection.

- Additive White Gaussian Noise (AWGN)

The AWGN Channel block models symbol errors resulting from a noisy propagation channel. It adds white Gaussian noise to a real or complex input signal. If the input signal is real, the block adds real white Gaussian noise to produce a real output signal. If the input signal is complex, the block adds complex white Gaussian noise to produce a complex output signal.

- Orthogonal Space-Time Block Code (OSTBC) Decoder

The Orthogonal Space-Time Block Codes (OSTBC) Decoder stage combines the received signals from all the receiving antennas and the Channel State Information (CSI) to recover the information of the symbols encoded by the OSTBC encoder.

- Quadrature Phase Shift Keying (QPSK) Demodulator

The QPSK Demodulator block demodulates the signal from the OSTBC Decoder and recovers the original data.

- Frame Error Rate (FER)

The Frame Error Rate Calculator works out the system FER by comparing the demodulated bits with the original bits sent per frame, to detect errors. It calculates the error rate as a running statistic, by dividing the total number of unequal pairs of data elements by the total number of input data elements from one source.

3.10 Conclusion

In this chapter, the mathematical model for an OSTBC MIMO transceiver in a Rayleigh fading channel is presented. This mathematical model is used to develop a Simulink model in Matlab. The model consists of a Random binary generator, QPSK Modulator, OSTBC Encoder, Rayleigh fading channel, AWGN channel, OSTBC Decoder and a QPSK Demodulator. This model can be used by radio engineering designers to model an OSTBC MIMO transceiver over a fading irregular terrain environment to determine the performance of a radio link. Even though there has not been a model on software that can precisely depict the real-time environment and behaviour of the channel, because of its unpredictable nature and unique physical attributes, this model however, attempts to achieve as much exactness as possible.

CHAPTER 4: SIMULATION RESULTS AND DISCUSSION

4.1 Introduction

This chapter presents simulation results based on the OSTBC MIMO transceiver system model developed in Chapter 3 using the Matlab/Simulink software program. This chapter aimed at examining the validity of the developed model and whether it can operate optimally with increased Signal-to-Noise Ratio (SNR) in a fading irregular terrain environment. This was done by analysing the Bit Error Rate (BER) results of the OSTBC MIMO system when four different MIMO antenna arrays are employed at both the transmitter and the receiver. Also, in this chapter, a radio link path into Henkriesmond Substation is proposed. The implementation of three different VHF frequencies was conducted on the proposed radio link's propagation prediction and Receive Signal Strength (RSS) results. The different simulations were conducted to investigate:

- Whether the BER could be reduced significantly to improve link performance, by employing the OSTBC MIMO transceiver system.
- Whether the Receive Signal Strength (RSS) could be improved significantly by employing the OSTBC MIMO system in the low VHF frequency band.

The following shows scenarios of $(BER, E_b/N_0)$ simulations, for different OSTBC MIMO transceiver systems, which were conducted:

- The first case scenario: 1 x 1 Single-In Single-Out (SISO) transceiver system.
- The second case scenario: 2 x 2 OSTBC MIMO transceiver system.
- The third case scenario: 3 x 3 OSTBC MIMO transceiver system.
- Finally, the fourth case scenario: 4 x 4 OSTBC MIMO transceiver system.

All the simulation scenarios are performed in a Rayleigh fading channel using the MATLAB/Simulink software. Section 4.3 shows the proposed Repeater coverage plot profiles to Henkriesmond Substation, operating at three different VHF frequency bands namely, 135 MHz, 100 MHz and 70 MHz.

The results show an improved SNR, with increased signal strength reception as the number of antennas used increases. The simulation results do show that the use of multiple antennas in the OSTBC MIMO transceiver system at the low VHF frequency band, yields significant improvements in the radio link performance in irregular terrain.

4.2 Simulation Results

4.2.1 First Case Scenario: Performance of a 1x1 SISO System in a Rayleigh Fading Channel

Figure 4.1 shows the simulation results from Matlab of a (BER vs E_b/N_0) curve based on the performance achieved across a 1x1 SISO transceiver system. The number of transmitting (Nt) and receiving (Nr) antennas used is 1 respectively.

Based on ($BER, E_b/N_0$) curve diagram shown in Figure 4.1, as the signal (E_b/N_0) increases, the bit error rate (BER) gradually shows a very slight but noticeable decrease as seen in Table 4.1.

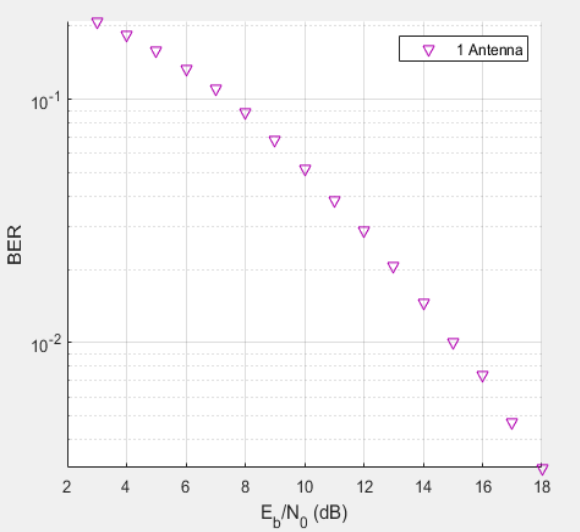

Figure 4. 1: The BER curve of a 1x1 SISO System

TABLE 4. 1: BER VALUES OF A 1X1 SISO SYSTEM IN A RAYLEIGH FADING CHANNEL.

E_b/N_0 (dB)	Bit Error Rate (BER)	Number of Bits
1	0.0	0
2	0.0	0
3	0.21	3000
4	0.1835	3000
5	0.1581	3000
6	0.1338	3000
7	0.1109	3000
8	0.0881	3000
9	0.0681	3000
10	0.0517	3000
11	0.0386	3000
12	0.0288	3000
13	0.0206	3000
14	0.0145	3000
15	0.01	3000
16	0.0073	3000
17	0.0047	3000
18	0.0030	3000

Based on the 1x1 SISO $(BER, E_b/N_0)$ curve diagram in Figure 4.1, assuming that the system is operating at $100Mb/s$, that is 10^8 bits per second. A discrete minimum BER reading that we can choose is at 15 dB (E_b/N_0) which is 10^{-2}, according to Figure 4.1. This means, 1-bit error occurs every 10^2 bits. Therefore, the time taken to receive 10^2 bits, would be:

$$\frac{Number\ of\ Bits\ Sent}{Bit\ Rate} = \frac{10^2}{10^8} = 1\mu s. \qquad (4.1)$$

This implies that $1\mu s$ is the average time it would take before an error can occur in this system. Therefore, we can see with the use of 1 antenna at both ends of the system that the radio link performance is very poor with errors occurring at every micro second.

The $(BER, E_b/N_0)$ curve diagram in Figure 4.1, shows the radio link performance achieved using the 1x1 SISO system, which is typical of the current radio link between Vioolstdrift Radio Site and Henkriesmond Substation in the Northern Cape Province.

4.2.2 Second Case Scenario: Performance of a 2x2 OSTBC MIMO System in a Rayleigh Fading Channel

In the second case scenario, Figure 4.2 shows the simulation results from Matlab of a (BER vs E_b/N_0) curve based on the performance achieved across a 2x2 OSTBC MIMO transceiver system. The number of transmitting (Nt)and receiving (Nr) antennas used is 2 respectively. Based on ($BER, E_b/N_0$) curve diagram shown in Figure 4.2, as the signal (E_b/N_0) increases, the bit error rate (BER) gradually shows a slight decrease when compared to figures in Table 4.1.

Based on the 2x2 OSTBC SISO ($BER, E_b/N_0$) curve diagram in Figure 4.2, still assuming that the system is operating at $100Mb/s$, which is 10^8 bits per second. According to Figure 4.2, the discrete minimum BER reading we can easily select is at 16 dB (E_b/N_0), which is approximately 10^{-3}. This means that 1-bit error occurs every 10^3 bits. Therefore, the time it would take to receive 10^3 bits before an error occurred would be approximately:

$$\frac{Number\ of\ Bits\ Sent}{Bit\ Rate} = \frac{10^3}{10^8} = 0.01ms. \qquad (4.2)$$

Therefore, $0.01ms$ is the average time it would take before an error could occur in this system. Hence, we can deduce that the use of 2 antennas at both ends of the system yields an improvement in performance compared to the 1x1 SISO system. In this radio link the performance is still poor, however, bit errors do not occur as frequently as in the 1x1 SISO system, the improvement is 0.1s.

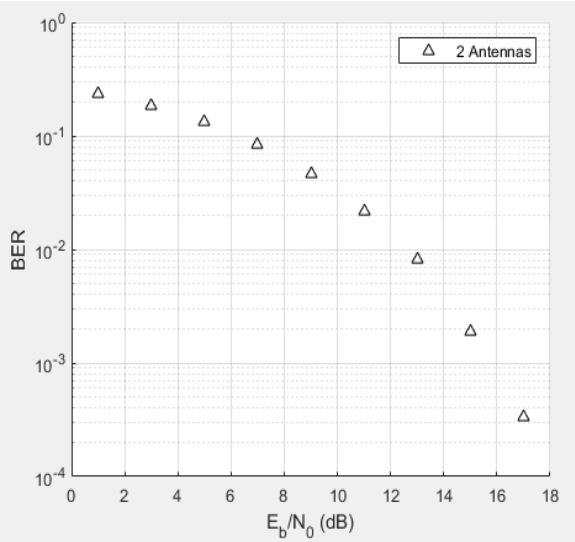

Figure 4. 2: The BER curve of a 2x2 OSTBC MIMO System

TABLE 4. 2: BER VALUES OF A 2X2 OSTBC MIMO SYSTEM (NT =2, NR =2) IN A RAYLEIGH FADING CHANNEL

E_b/N_0 (dB)	Bit Error Rate (BER)	Number of Bits
1	0.0	0
2	0.0	0
3	0.1845	3000
4	0.1589	3000
5	0.1330	3000
6	0.1080	3000
7	0.0847	3000
8	0.0637	3000
9	0.0468	3000
10	0.0318	3000
11	0.0214	3000
12	0.0132	3000
13	0.0080	3000
14	0.0042	3000
15	0.0019	3000
16	0.000733	3000
17	0.000333	3000
18	0.0000333	3000

4.2.3 Third Case Scenario: Performance of a 3x3 OSTBC MIMO System in a Rayleigh Fading Channel

The third case scenario are simulation results from Matlab of a (BER vs E_b/N_0) curve based on the performance achieved across the 3x3 OSTBC MIMO transceiver system as shown in Figure 4.3. The number of transmitting (Nt) and receiving (Nr) antennas used in this scenario is 3 respectively. Based on ($BER, E_b/N_0$) curve diagram shown in Figure 4.3, as the signal (E_b/N_0) increases, the bit error rate (BER) shows an improved decrease compared to Figures 4.1 and 4.2.

Based on the 3x3 OSTBC MIMO ($BER, E_b/N_0$) curve diagram in Figure 4.3, again assuming that the system is operating at $100Mb/s$, which is 10^8 bits per second. According to Figure 4.3, the discrete minimum BER reading is at 16 dB (E_b/N_0), which is 10^{-4}. This means that 1-bit error occurs every 10^4 bits in this system. Therefore, the time taken to receive 10^4 bits before an error occurs, would approximately be:

$$\frac{Number\ of\ Bits\ Sent}{Bit\ Rate} = \frac{10^4}{10^8} = 0.1ms. \qquad (4.3)$$

Therefore, $0.1ms$ is the average time it would take before an error could occur in this system. Therefore, we see that the use of 3 antennas at each end of the system drastically improves the performance the system. In the third scenario, the radio link performance has shown much improvement than in the first or second scenario.

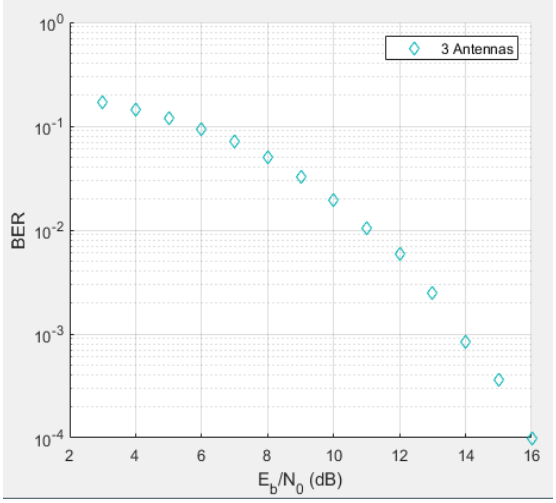

Figure 4. 3: The BER curve of a 3x3 OSTBC MIMO System

TABLE 4. 3: BER VALUES OF A 3X3 OSTBC MIMO SYSTEM (NT=3, NR=3) IN A RAYLEIGH FADING CHANNEL

E_b/N_0 (dB)	Bit Error Rate (BER)	Number of Bits
1	0.0	0
2	0.0	0
3	0.1718	3000
4	0.1438	3000
5	0.1205	3000
6	0.0942	3000
7	0.0710	3000
8	0.0500	3000
9	0.0324	3000
10	0.0195	3000
11	0.0103	3000
12	0.0058	3000
13	0.0025	3000
14	0.000833	3000
15	0.000366	3000
16	0.0001	3000
17	0.0	3000
18	0.0	3000

4.2.4 Fourth Case Scenario: Performance of a 4x4 OSTBC MIMO System in a Rayleigh Fading Channel

The fourth case scenario shown in Figure 4.4, are simulation results from Matlab of a (BER vs E_b/N_0) curve based on the performance achieved across a 4x4 OSTBC MIMO transceiver system. The number of transmitting (Nt)and receiving (Nr) antennas used in this scenario are 4 respectively. Based on ($BER, E_b/N_0$) curve diagram shown in Figure 4.4, as the signal (E_b/N_0) increases, the bit error rate (BER) shows a more significant decrease to that seen in Figures 4.1, 4.2 and 4.3.

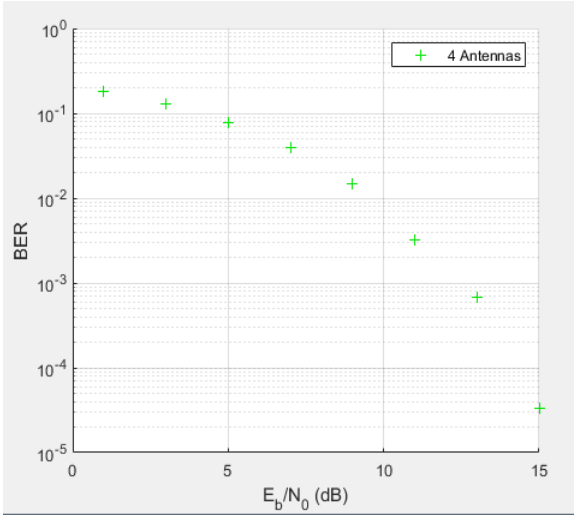

Figure 4. 4: The BER curve of a 4x4 OSTBC MIMO System

TABLE 4. 4: BER VALUES OF A 4X4 OSTBC MIMO SYSTEM (NT=4, NR=4) IN A RAYLEIGH FADING CHANNEL

E_b/N_0 (dB)	Bit Error Rate (BER)	Number of Bits
1	0.0	0
2	0.0	0
3	0.1267	3000
4	0.1009	3000
5	0.0784	3000
6	0.0580	3000
7	0.0395	3000
8	0.0252	3000
9	0.0147	3000
10	0.0078	3000
11	0.0032	3000
12	0.0019	3000
13	0.000666	3000
14	0.000133	3000
15	0.0000366	3000
16	0.0000366	3000
17	0.0	3000
18	0.0	3000

Based on the 4x4 OSTBC MIMO ($BER, E_b/N_0$) curve diagram in Figure 4.4, again assuming that the system is operating at $100Mb/s$, which is 10^8 bits per second. According to Figure 4.4, the minimum discrete BER reading is found at 18 dB (E_b/N_0), which is 10^{-5}. This means that 1-bit error occurs every 10^5 bits. Therefore, to receive 10^5 bits before an error could occur in this system, the time taken would be approximately:

$$\frac{Number\ of\ Bits\ Sent}{Bit\ Rate} = \frac{10^5}{10^8} = 1ms. \qquad (4.4)$$

Therefore, $1ms$ is the average time it would take before an error could occur in this system. This affirms that the use of 4 antennas at both ends of the system, greatly improves the performance of the system. In this scenario, the radio link performance is far better than any of the previously mentioned scenarios.

4.2.5 BER Results for all 4 Systems in a Rayleigh Fading Channel

Figure 4.5 is a $(BER, E_b/N_0)$ curve diagram displaying all four transceiver system results in one graph. From Figures 4.1 through to 4.4, it is evident that the bit error rate decreases as the number of antennas used increases, thus improving the quality of the wireless communication channel.

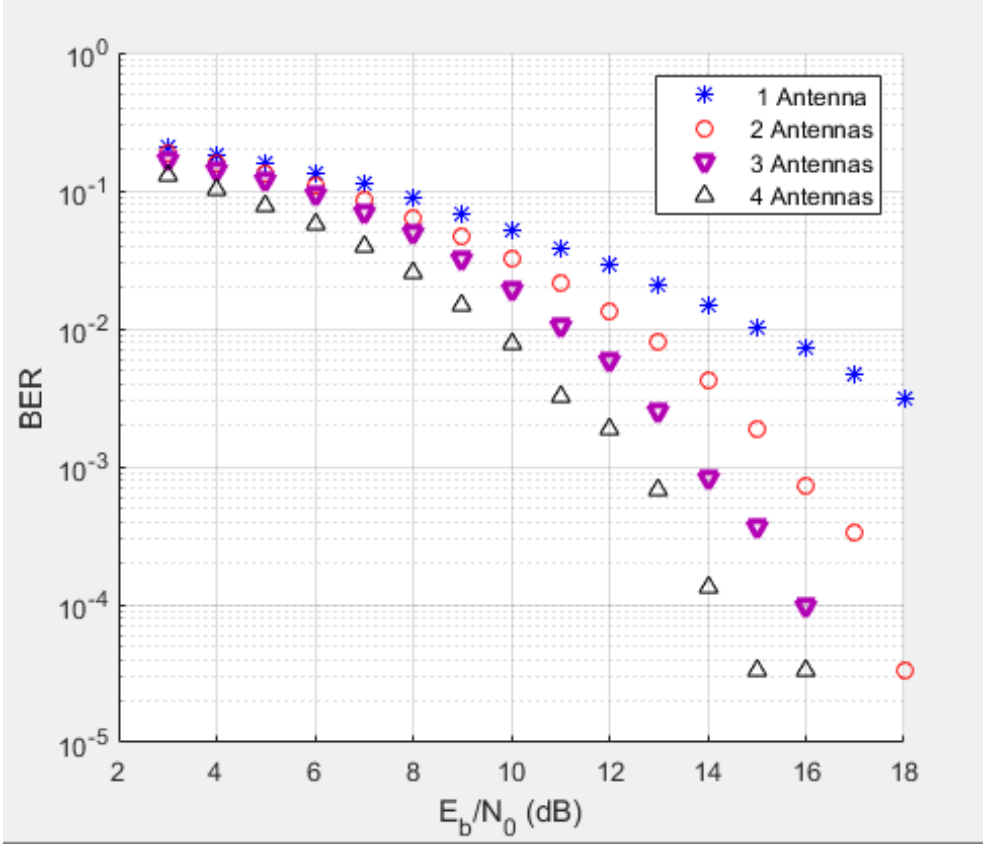

Figure 4. 5: The BER curve for all 4 Systems

The simulation results received confirm that Shannon's Law is true. Shannon's Law governs the amount of data that can be passed in a channel in the presence of noise. Shannon's Law is represented by the following equation:

$$C = W \log_2(1 + S/N) \quad (4.5)$$

Where:

C = Channel capacity($^{b}/_{s}$)

W = Bandwidth (Hz)

$^{S}/_{N}$ = Signal to Noise Ratio (dB)

With the use of the MIMO technology, the capacity of the channel increases as shown by the following equation:

$$C = N.W \log_2(1 + {}^{S}/_{N}) \quad (4.6)$$

Where:

N = Number of antennas used

An increase in the number of antennas used results in greater channel capacity. Therefore, the use of multiple antennas could yield infinite channel capacity, while reducing bit error rate (BER) and improving signal to noise ratio (SNR).

4.3 Proposed Radio Link Path into Henkriesmond Substation in the Northern Cape

4.3.1 Proposed Radio Link Path into Henkriesmond Substation

Figure 4.6 shows a proposed radio link path into Henkriesmond Substation. The proposed radio path consists of a microwave radio link between Vioolsdrift Radio Site and Doringwater Substation, and a VHF Repeater at Doringwater Substation propagating towards Henkriesmond Substation. The Repeater at Doringwater Substation has a 12 element Yagi antenna at a height of 60m. Three different VHF frequency bands namely, 135 MHz, 100 MHz and 70 MHz were exploited. The distance between the transmitter and receiver is 11km. The interfering obstacle (mountain) is 700m above sea-level. This portion of the study focuses on the radio signal propagation performance of the VHF Repeater at Doringwater Substation towards Henkriesmond Substation (Figure 4.7). The design of the microwave link from Vioolsdrift Radio Site to Doringwater Substation will not be dealt with in this study.

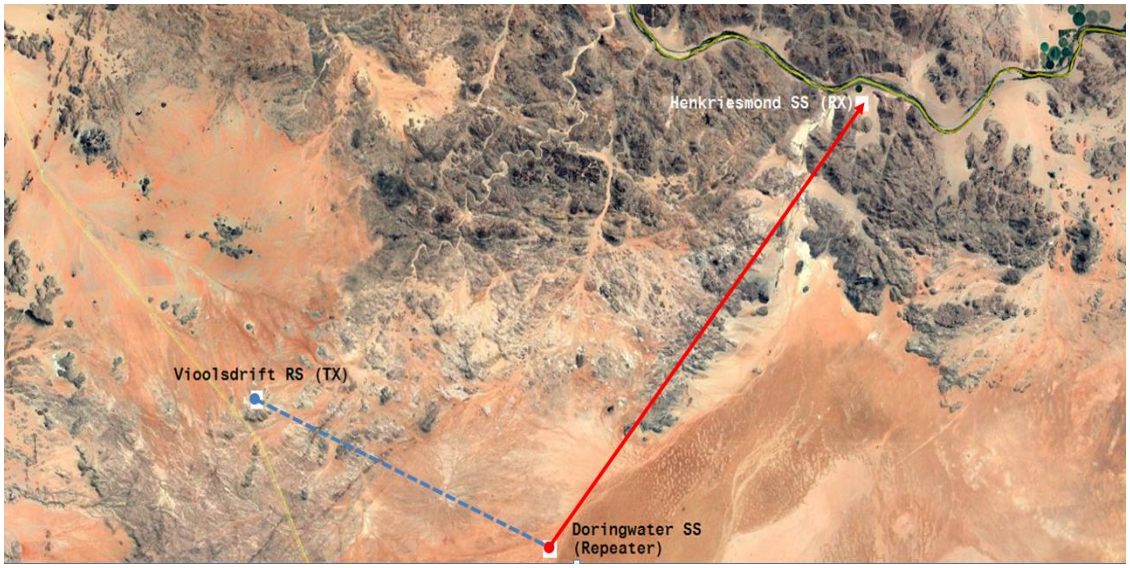

Figure 4. 6: Google Earth Image of the Proposed Radio Link Path into Henkriesmond Substation

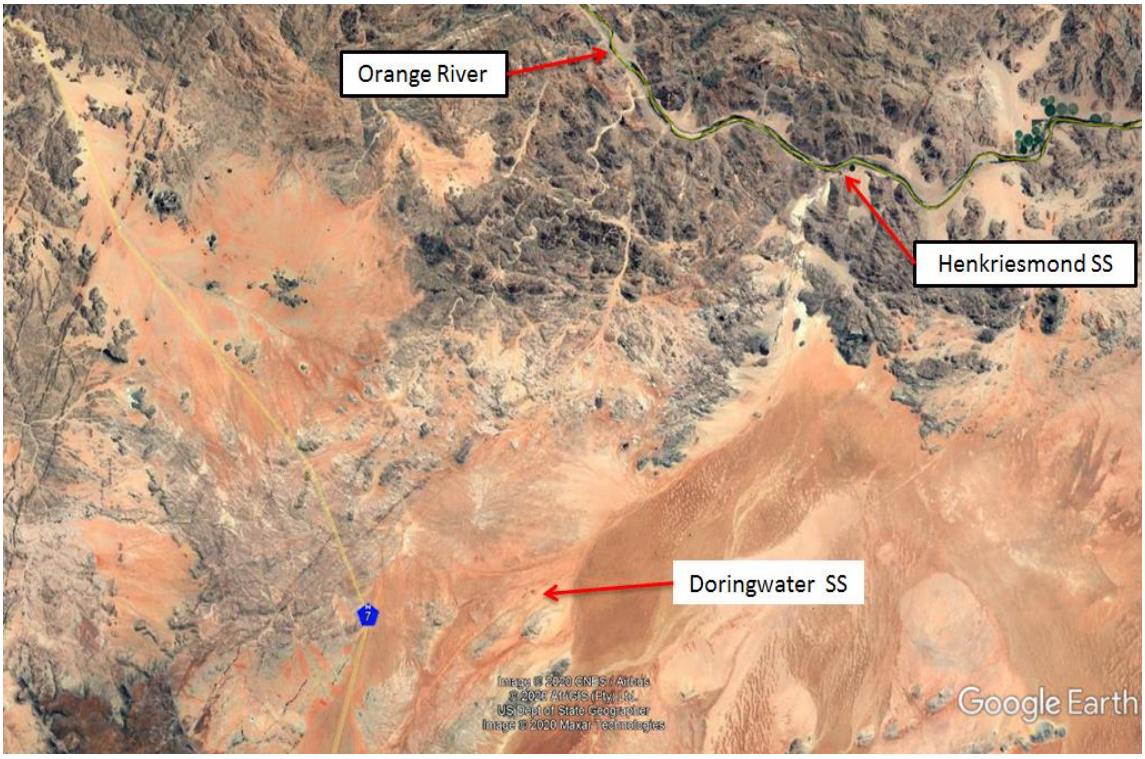

Figure 4. 7: Google Earth Image of the Location of Doringwater Substation and Henkriesmond Substation

4.3.2 A 4x4 OSTBC MIMO System Operating at a VHF Frequency of 135 MHz

Figure 4.8 is a simulated Matlab SiteViewer propagation pattern for a VHF OSTBC MIMO repeater situated at the transmitting site (TX) Doringwater Substation, propagating towards the receiving site (RX) Henkriesmond Substation operating at a frequency of 135 MHz. Table 4.5, which comprises the propagation profile of this Repeater, shows the Receive Signal Strength (RSS) level of this system as -96.92 dBm. This level reading indicates that the RTU at Henkriesmond Substation would fail at -96.92dBm, because this level is too weak for reliable data transmission. The standard Receive Signal Strength (RSS) level threshold for RTU operation at Eskom is -90 dBm [67].

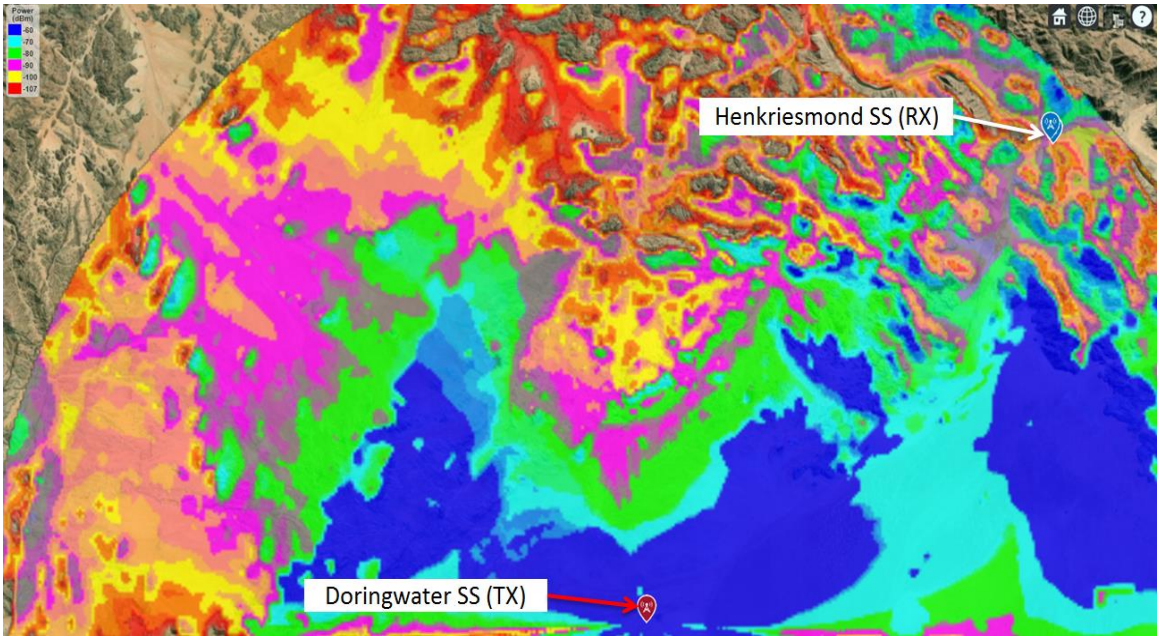

Figure 4. 8: Matlab SiteViewer Propagation Diagram to Henkriesmond Substation Operating at 135 MHz

TABLE 4. 5: PROPAGATION PROFILE OF THE VHF REPEATER TO HENKRIESMOND SUBSTATION AT 135MHZ

Doringwater Substation (TX)	**Parameters**
Latitude	-29.08333333
Longitude	17.94527778
Frequency (MHz)	135
TX power (watts)	10
Elevation (m)	700
Antenna height (m)	60
Antenna model	Yagi (12 El) Y425_12
Antenna gain (dBi)	16
MIMO Array	4 x 4
Azimuth (°)	30
Henkriesmond Substation (RX)	
Latitude	-28.90111111
Longitude	18.13694444
Antenna model	Yagi (12 El) Y425_12
Antenna height (m)	60
RX Sensitivity Criteria (dBm)	-90
RX Sensitivity (dBm)	-107
RX Signal Strength (dBm)	**-96.92**

4.3.3 A 4x4 OSTBC MIMO System Operating at a VHF Frequency of 100 MHz

Figure 4.9 is a simulated Matlab SiteViewer propagation pattern similar to Figure 4.8 except that its operating frequency is 100 MHz. Again, when looking at the readings in Table 4.6, which contains the propagation profile for this Repeater, the Receive Signal Strength (RSS) of this system has now greatly improved to -90.53 dBm. This reading indicates that the RTU at Henkriesmond Substation would work marginally at -90.53dBm, because the usable receive signal strength (RSS) level threshold for RTU operation at Eskom is -90 dBm [67].

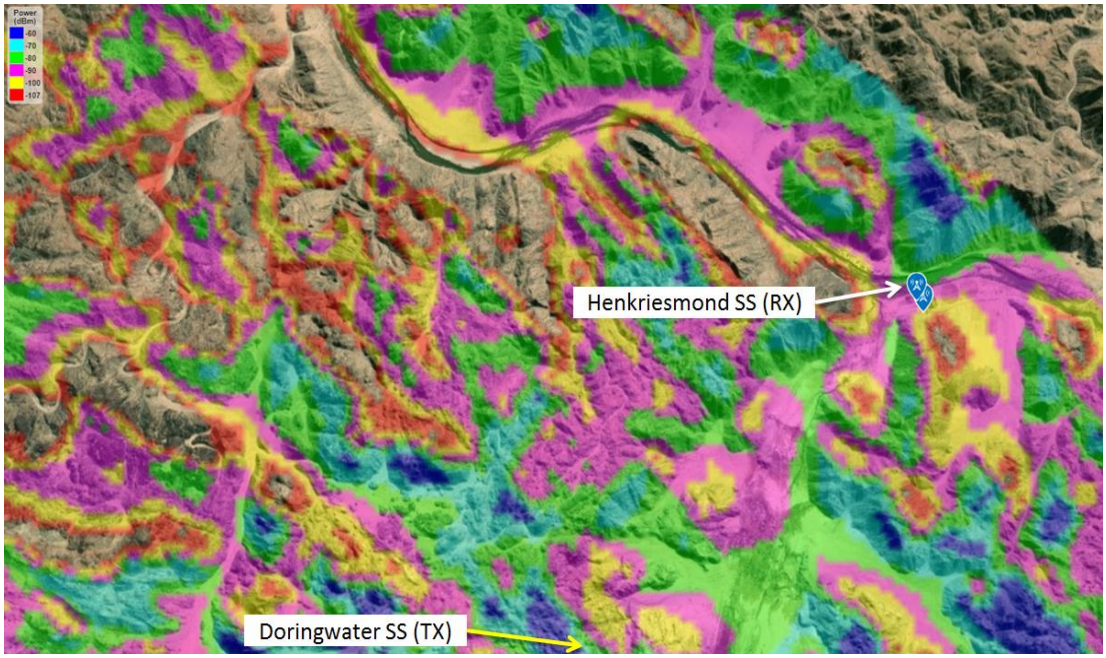

Figure 4. 9: Matlab SiteViewer Propagation Diagram to Henkriesmond Substation Operating at 100 MHz

TABLE 4. 6: PROPAGATION PROFILE OF THE VHF REPEATER TO HENKRIESMOND SUBSTATION AT 100MHZ

Doringwater Substation (RX)	**Parameters**
Latitude	-29.08333333
Longitude	17.94527778
Frequency (MHz)	100
TX power (watts)	10
Elevation (m)	700
Antenna height (m)	60
Antenna model	Yagi (12 El) Y425_12
Antenna gain (dBi)	16
MIMO Array	4 x 4
Azimuth (°)	30
Henkriesmond Substation (TX)	
Latitude	-28.90111111
Longitude	18.13694444
Antenna model	Yagi (12 El) Y425_12
Antenna height (m)	60
RX Sensitivity Criteria (dBm)	-90
RX Sensitivity (dBm)	-107
RX Signal Strength (dBm)	**-90.53**

4.3.4 A 4x4 OSTBC MIMO System Operating at a VHF Frequency of 70 MHz

Figure 4.10 is also a simulated Matlab SiteViewer propagation pattern similar to Figures 4.8 and 4.9 except that its operating frequency is much lower at 70 MHz. The Receive Signal Strength (RSS) reading of this system in Table 4.7, has improved beyond the threshold to -89.71dBm. This reading indicates that the RTU at Henkriesmond Substation would operate at -89.71dBm, because it is within the usable receive signal strength (RSS) level of -90 dBm [67].

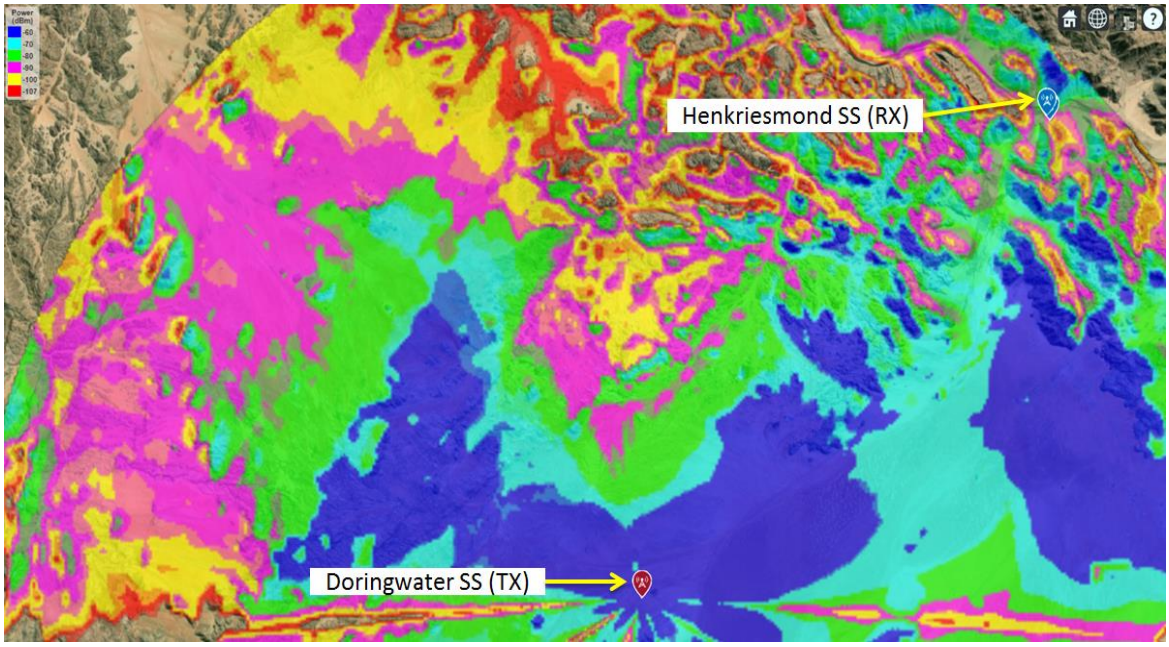

Figure 4. 10: Matlab SiteViewer Propagation Diagram to Henkriesmond Substation Operating at 70 MHz

TABLE 4. 7: PROPAGATION PROFILE OF THE VHF REPEATER TO HENKRIESMOND SUBSTATION AT 70MHZ

Doringwater Substation (TX)	**Parameters**
Latitude	-29.08333333
Longitude	17.94527778
Frequency (MHz)	70
TX power (watts)	10
Elevation (m)	700
Antenna height (m)	60
Antenna model	Yagi (12 El) Y425_12
Antenna gain (dBi)	16
MIMO Array	4 x 4

Azimuth (°)	30
Henkriesmond Substation (RX)	
Latitude	-28.90111111
Longitude	18.13694444
Antenna model	Yagi (12 El) Y425_12
Antenna height (m)	60
RX Sensitivity Criteria (dBm)	-90
RX Sensitivity (dBm)	-107
RX Signal Strength (dBm)	**-89.71**

The simulation results obtained in this section confirm that the OSTBC MIMO system operated at the low VHF frequency band does mitigate radio signal reflection, fading and scattering. The VHF OSTBC MIMO system employed in mountainous terrain does provide a quality communication channel compared to a single antenna transceiver.

4.4 Conclusion

This chapter has demonstrated various simulation results. The results illustrate that employing the 4x4 OSTBC MIMO system does greatly improve the recovery of the transmitted signal at the receiver. Also, the use of the OSTBC MIMO system at low VHF frequencies further improves signal reception in irregular terrain environments.

CHAPTER 5: CONCLUSION AND FUTURE STUDIES

5.1 Conclusion

This chapter provides a conclusion on the use of an OSTBC MIMO transceiver at the low VHF frequency band, resulting in better signal reception in irregular terrain environments. A broad search was applied to other forms of transceivers and modulation schemes, as a means of revealing a proper selection of technologies suitable for irregular terrain use.

The principle of the OSTBC and MIMO technologies have been presented in Chapter 2, which outlined the benefits of their use as improved signal-to-noise ratio (SNR), and increased data rate and channel capacity. The emphasis was on reviewing the use of the MIMO technology at the low VHF frequency band (49-108 MHz) to achieve diffraction of the radio signals over mountainous terrain. This research also exposed the fact that there is an opportunity to increase data rates even at lower frequencies by applying a high order modulation scheme such as QPSK with the MIMO technology.

In Chapter 3, the development of a mathematical model for the OSTBC MIMO was done to demonstrate how the different components of the transceiver in a fading channel function and link to one another.

In Chapter 4, using MATLAB/Simulink software package, various simulation cases were developed. The simulation results confirmed that using multiple antenna arrays reduces bit errors and yields an improved signal to noise ratio (SNR) in a fading radio communication channel. In addition, the use of the low VHF frequency band with OSTBC MIMO greatly increases radio signal reception in mountainous terrains. Three different VHF frequencies were explored namely: 135 MHz, 100 MHz and 70 MHz. The lowest frequency proved to be the best option to consider in mountainous terrain.

The developed model and simulation cases have also been used to:

- Analyse the relationship between the variation of the number of antennas used and the Bit Error Rate (BER).

- Analyse the relationship between the variation of the number of antennas used and the Eb/No.
- Analyse the relationship between different low frequency values within the VHF band and their diffraction abilities over mountainous terrain.
- Demonstrate the potency and the need for the VHF OSTBC MIMO system to be considered for radio communication in mountainous terrain by different sectors that make use of radio communication including Eskom.

5.2 Suggestions for Further Studies

For future research, the developed VHF OSTBC MIMO model will be implemented as a physical prototype to validate the developed model and the simulation results.

REFERENCES

[1] S. Dludla, Agribusiness Opportunities in Northern Provinces, pp. 1 [Online] Available at: https://www.smesouthafrica.co.za/Agribusiness-opportunities-in-northern-provinces/ [Accessed: 19 September 2020].

[2] J. H. Wellington, P. S. Hattingh and J. Cooks, Orange River - South Africa, pp.1 [Online] Available at: https://www.britannica.com/place/Orange-River [Accessed: 19 September 2020].

[3] P. Zhang and Z. Zhao, "Design of SCADA power Distribution Monitoring System based on PLC and Configuration Software", in: International Conference on Mechanical Engineering and Material Science, pp. 152, 2012.

[4] G. B. Silberbauer and R. F. Logan, Kalahari Desert, Desert Region, Africa, pp. 2, [Online] Available at: https://www.britannica.com/place/Kalahari-Desert [Accessed: 19 September 2020].

[5] M. D. Casciato, "Radio Wave Diffraction and Scattering Models for Wireless Channel Simulation", Ph.D. dissertation, Electrical Engineering, The University of Michigan, pp.1-2, 2001.

[6] G. Breed, "Bit Error Rate: Fundamental Concepts and Measurement Issues", *High Frequency Electronics*, pp. 46, 2003.

[7] B, Stec and W. Susek, Theory and Measurement of Signal-to-Noise Ratio in Continuous-Wave Noise Radar, Faculty of Electronics, Military University of Technology, Gen. Urbanowicz St. No 2, 00-908 Warsaw, Poland, pp. 1, 6 May 2018.

[8] T. Wu, T. S. Rappaport and C. M. Collins, "The Human Body and Millimeter-Wave Wireless Communication Systems: Interactions and Implications", in IEEE International Conference on Communications (ICC), pp. 1-3, June 2015.

[9] H. Sizu, *Radio Wave Propagation for Telecommunication Applications*, pp. 49-51, 2003.

[10] J, S. Seybold, *Introduction to RF Propagation*, pp. 54, 2005.

[11] I. Poole, Electromagnetic waves - reflection, refraction, diffraction, pp. 2. [Online] Available at: http://www.radio- electronics.com/ info/propagation/em_waves/ electromagnetic-reflection-refraction- diffraction.php [Accessed: 19 September 2020].

[12] S. N. Ghosh, *Electromagnetic Theory and Wave Propagation*, pp. 89, 2002.

[13] X. B. Maxama and E. D. Markus, “A survey on propagation challenges in Wireless Communication Networks over Irregular Terrains”, in: Open Innovations IEEE Conference, pp. 1, October 2018.

[14] L. Michalek, M. Dvorsky, O. Grunt, J. Skapa and R. Sebesta, Analysis of Signal Attenuation in UHF Band, *Information and Communication Technologies, and Services*, vol. 13, no. 4, pp. 338, 2015.

[15] K. O. Suleman, I. T. Bello, L. O. Tijani, A. O. Ogunbode and W. A. Olayiwola, Effect of Temperature and Ground Water on VHF Radio Wave Propagation in Tropical Climate, *International Journal of Scientific & Engineering Research*, vol. 8, no. 1, pp. 1391-1394, January 2017.

[16] J. Zang and X. Wang, Measurements and Modeling of Path Loss over Irregular Terrain for Near-Ground and Short-Range Communications, *Progress in Electromagnetics Research M*, vol. 57, pp. 55–62, 2017.

[17] J. Yuansheng, Signal Designs for MIMO-OFDM Systems, Doctoral Dissertations, University of Delaware, 2017.

[18] Z. Naseem, I. Nausheen, Z. Mirza, Propagation Models for Wireless Communication System, *International Research Journal of Engineering and Technology (IRJET)*, vol. 5, no. 01, pp. 237-238, January 2018.

[19] S. Arvind and V. D. Mytri, Design of Simulink Model for OSTBC and Performance Evaluation of IEEE 802.16 OFDM Physical Link with and without Space-Time Block Coding for Wireless Communication, IJERA, pp. 9, 9-10 January 2015.

[20] Space Weather Services, Introduction to HF Radio Propagation, Australian Government, pp. 18, 2016.

[21] H. Sizu, *Radio Wave Propagation for Telecommunication Applications*, pp. 49-51, 2003.

[22] J. S. Seybold, *Introduction to RF Propagation*, pp. 54, 2005.

[23] S. N. Ghosh, *Electromagnetic Theory and Wave Propagation*, pp. 89, 2002.

[24] Federal Communications Commission, Revitalization of the AM Radio Service, Notice of Proposed Rulemaking, FCC 15-142, 30 FCC Rcd 12145, pp. 3, 23 October 2015.

[25] J. F. Coll, Channel Characterization and Wireless Communication Performance in Industrial Environments, Ph.D dissertation, Information and Communication Technology Stockholm, Sweden, pp. i, June 2014.

[26] Space Weather Canada, Geomagnetic Effects on Radio Propagation, pp. 1, [Online] Available at: http://www.spaceweather.gc.ca/tech/se-hf-en.php [Accessed: 15 April 2020].

[27] J. Luomala and I. Hakala, "Effects of Temperature and Humidity on Radio Signal Strength in Outdoor Wireless Sensor Networks", in: Proceedings of the Federated Conference on Computer Science and Information Systems, vol. 5, pp. 1247–1255, 2015.

[28] J. A. Boan, Radio Propagation in Fire Environments, Ph.D. dissertation, University of Adelaide, School of Electrical and Electronic Engineering, pp. 1-2, 2009. [28]. Gerini Yannick, Shortwave propagation and communication systems, pp. 1, 2001.

[29] N. Blaunstein, D. Censor, and D. Katz, Radio Propagation in Rural Residential Areas With Vegetation, *Progress In Electromagnetics Research,* PIER 40, pp. 132, 2003.

[30] C. He, C. T. X Li, C. Zhang, S. Zhang, and C. Liu, A Channel Estimation Scheme for MIMO-OFDM Systems, *IOP Conf. Series: Journal of Physics: Conf. Series,* 887, pp.1, 2017.

[31] J. Yuansheng, Signal Designs for MIMO-OFDM Systems, Ph.D dissertation, University of Delaware, 2017.

[32] R. C. Daniels and S. W. Peters, *A New MIMO HF Data Link: Designing for High Data Rates and Backwards Compatibility,* pp.1, 2013.

[33] A. Kumar and R. Bahl, An Architecture for High Data Rate Very Low Frequency Communication, *Defence Journal,* vol.63, no.1, pp. 25, January 2013.

[34] V. Gopinath and N. Krishnas, Enhanced Performance of HF OFDM in Wireless Communication, *Kiet International Journal of Communication and Electronics,* vol. 2, no.1, pp. 46, January-April 2014.

[35] H. D. Tuan, D. Ngo and H. H. M. Tam, Joint Power Allocation for MIMO-OFDM Full-Duplex Relaying Communications, *EURASIP,* pp. 19, 19 January 2017.

[36] J. Xu, D. L. Goeckel, and R. Janaswamy, The Capacity of MIMO Systems with Increasing SNR by Electromagnetic Analysis, *IEEE Transaction On Wireless Communication,* vol. 8, no. 9, September 2009.

[37] J. R. Champion, An Empirical Investigation of High Frequency Ground Wave Propagation, *John Hopkins APL Technical Digest,* vol. 13, no. 4, pp. 517, 1992.

[38] Space Weather Services, Introduction to HF Radio Propagation, Australian Government, pp. 10, 2016.

[39] H. Sizu, *Radio Wave Propagation for Telecommunication Applications,* pp. 49-51, 2003.

[40] A. Kumar and R. Bahl, An Architecture for High Data Rate Very Low Frequency Communication, *Defence Journal*, vol. 63, no.1, pp. 26, January 2013.

[41] Veena Gopinath and Nitha Krishnas, Enhanced Performance of HF OFDM in Wireless Communication, Kiet International Journal of Communication and Electronics, Vol. No.2, Issue No.1, pp. 46, Jan-April 2014.

[42] M. Yahyaoui, A. Moussati and G. Zein, On the Capacity of MIMO-OFDM based Diversity and Spatial Multiplexing in Radio-over Fibre System, Optics Communications, Vol. 402, pp.252, Nov. 2017.

[43] Chunlong He, Chu Tian, Xingquan Li, Ce Zhang, Shiqi Zhang, and Chaowen Liu, A Channel Estimation Scheme for MIMO-OFDM Systems, IOP Conf. Series: Journal of Physics: Conf. Series 887, pp.1, 2017.

[44] Richard Van Nee, V.K. Jones, Geert AWater, Allet Van Zelst, James Gardner and Greg Steele, The 802.11n MIMO-OFDM Standard for Wireless LAN and Beyond, pp. 445, 2006.

[45] J. Yuansheng, Signal Designs for MIMO-OFDM Systems, Doctoral Dissertations, University of Delaware, 2017.

[46] H.D. Tuan, D. Ngo and H. H.M. Tam, Joint Power Allocation for MIMO-OFDM Full-Duplex Relaying Communications, EURASIP, pp. 19, 19 Jan 2017.

[47] Jie Xu, Dennis L. Goeckel, and Ramakrishna Janaswamy, The Capacity of MIMO Systems with Increasing SNR by Electromagnetic Analysis, IEEE Transaction on Wireless Communication, Vol. 8, No. 9, September 2009.

[48] R. Sharma, MTN Plan to Roll-out South Africa's Largest 4x4 MIMO Network this Year, pp. 1, [Online] Available at: http://www.thefastmode.com/technology-solutions/10328-mtn-plan-to-rollout-south-africas-largest-4x4-mimo-network-this-year [Accessed: 7 April 2020].

[49] S. Dogan, A. Tusha and H. Arslan, OFDM with Index Modulation for Asynchronous mMTC Networks, Sensors, Vol 18, No. 1280, pp. 2, 21 April 2018.

[50] IARU Region Maps, pp.1, [Online] Available at: http://www.mapability.com/ei8ic/maps/regions.php [Accessed: 20 March 2020].

[51] A. Goldsmith, *Wireless Communications*, 1st ed. Cambridge University Press: Cambridge, England, 2005.

[52] A. Al-Omary, End-to-End Performance Evaluation for MIMO-OSTBC Adaptive Modulation Over Rayleigh Fading Channel, *IJET*, pp. 8, 2018.

[53] N. Balaban and J. Salz, Dual Diversity Combining and Equalization in Digital Cellular Mobile Radio, *IEEE Trans. Veh. Technol.*, vol. 40, pp. 342-354, May 1991.

[54] G. J. Foschini Jr., Layered Space-Time Architecture for Wireless Communication in a Fading Environment when Using Multi-Element Antennas, Bell Lab Tech. J., pp. 41-59, 1996.

[55] G. J. Foschini Jr., and M. J. Grans, On Limits of Wireless Communication in a Fading Environment when using Multiple Antennas, Wireless Personal Communication, March 1998.

[56] V. Tarakh, H. Jafarkhani, A. R. Calderbank, Space-Time Block Code from Orthogonal Designs, IEEE, *Trans. Info. Theory*, vol. 45, no. 5, pp. 1456, 1999.

[57] T. Brown, E. De Carvalho and P. Kyritsi, *Practical Guide to the MIMO Radio Channel with MATLAB Examples*, pp. xi, 2012.

[58] J. S. Lu and H. L. Bertoni, "A Site-Specific MIMO channel Simulator for Hilly and Mountainous Environments", in: IEEE Military Communications Conference, pp. 764, 2013.

[59] H. Bolcskei and E. Zurich, *MIMO-OFDM Wireless Systems: Basics, Perspective, and Challenges*, pp. 33, August 2006.

[60] T.X. Lai and A.B. Sessay, "Performance Analysis of Space Time Block Coded Systems over Frequency Selective Rayleigh Fading Channels", in: IEEE Wireless Communications and Networking Conference, vol. 3, pp. 1480-1485, 2006.

[61] L. Cortes-Pena, MIMO Space-Time Block Coding: Simulation and Results, *E CE6604 Personal and Mobile Communications*, pp. 1-8, 2009.

[62] S. M. Alamouti, A Simple Transmitter Diversity Scheme for Wireless Communications, *IEEE J. Select. Areas Commun.*, vol. 16, pp. 1451-1458, October 1998.

[63] L. A. Perisoara, BER Analysis of STBC Codes for MIMO Rayleigh Flat Fading Channels, *Telfor Journal*, v. 4, no. 2, pp. 78, 2012.

[64] G. Genesan, and P. Stoica, Space-Time Block Codes: A Maximum SNR Approach, *IEEE Trans. Inform. Theory*, vol. 47, no. 4, pp.1650-1656, 2001.

[65] B. M. Hochwald, and T. L. Marzetta, Unitary Space-Time Modulation for Multiple-Antenna Communications in Rayleigh Flat Fading, *IEEE Trans. Inform. Theory*, vol. 46 no. 2, pp. 543-564, 2000.

[66] B. R. Ballal, A. Chadha and N. Satam, Orthogonal Frequency Division Multiplexing and its Applications, *IJSR*, vol. 2, no. 1, pp.325-328, January 2013.

[67] P. Delport, Optimisation of UHF Radio SCADA Systems for Electrical Distribution Networks, Master of Engineering Science Thesis, University of Stellenbosch, pp. 46-60 , April 2006.

[68] Q. Trio, Licenced VHF|UHF Ethernet and Serial Data Radio, pp.1 [Online] Available at: http://www.download.schneider-electric.com/trioq/radio [Accessed: 9 March 2020].

[69] B.R. Ballal, A. Chadha, N. Satam, Orthogonal Frequency Division Multiplexing and its Applications, International Journal of Science and Research, Vol 2, Issue 1, pp. 325-328, January 2013.

[70] A. S. Babu, D. A. Kumar, Performance Analysis of Orthogonal Space Time Block Code and Transmission Antenna Selection with Multi-User Diversity, *IJCSMC*, vol. 3, no. 8, pp. 361-366, August 2014.

[71] P. H. Bardell, W. H. McAnney, and J. Savir, "Built-In Test for VLSI: Pseudorandom Techniques", John Wiley & Sons: New York, 1987.

[72] Pseudorandom Binary Generators, pp.1, [Online] Available at: http://www.cs.miami.edu/home/burt/learning/Csc609.022/random_numbers.html [Accessed: 10 March 2020].

[73] A. Singh, V. Esham, S. Nargis, J. Sirisha, PRBS Generator Module, Lab Project, pp. 2, 2014.

[74] Pseudorandom Binary Sequence, pp.1, [Online] Available at: https://en.wikipedia.org/wiki/Pseudorandom_binary_sequence [Accessed: 10 March 2020].

[75] N. Laszlo, Articles on Correlation and Calibration, pp. 1, 11 November 2013.

[76] Mathuranathan, QPSK Modulation and Demodulation, pp.2-3, 19 October 2010.

[77] L. Teschler, QPSK Modulation and Generating Signals, pp.1,[Online] Available at: https://www.testandmeasurementtips.com/basics-qpsk-modulation-display-qpsk-signals/ [Accessed: 18 February 2020].

[78] Quadrature Phase Shift Keying, pp. 1, [Online] Available at: https://www.propagation.ece.gatech.edu/ECE6390/project/Fall2010/Projects/group6/ExoBuzz/page1/page8.html [Accessed: 10 March 2020].

[79] L. Govekar, Y. S. Rao, Implementation of an Adaptive MIMO System using Effective Minimization of Frame Error Rate, *IJITEE*, ISSN: 2278-3075, vol. 9, no. 4, pp. 2290-2294, February 2020.

[80] V. Tarokh, H. Jafarkhami, and A. R. Calderbank, Space-Time Block Codes from Orthogonal Designs, *IEEE Transactions on Information Theory*, vol. 45, no.5, pp. 1456-1467, 1999.

[81] Md. Golam Sadeque, S. C. Mohonta, Md. Firoj Ali, Modeling and Characterization of Different Types of Fading Channel, *IJSETR*, vol. 4, no. 5, pp. 1410-1415, May 2015.

[82] T. S. Rappaport, *Wireless Communications: Principles and Practice*, 2nd ed. Prentice Hall PTR, ISBN 978-0-13-042232-3, 31 December 2001.

[83] Additive White Gaussian Noise, pp. 1, [Online] Available at: https://www.en.m.wikipedia.org/awgn.html [Accessed: 11 March 2020].

[84] K. Sankar, Alamouti STBC with Two Receive Antenna, pp. 2-3, [Online] Available at: https://www.dsplog.com/2009/03/15/alamouti-stbc-2-receive-antenna/ [Accessed: 20 February 2020].

[85] R. Kumar, R Saxena, Performance Analysis of MIMO-STBC Systems with Higher Coding Rate using Adaptive Semiblind Channel Estimation Scheme, The Scientific World Journal, 2014.

[86] QPSK Modulation and Demodulation, pp. 2, [Online] Available at: http://www.gaussianwaves.com/2010/10/qpsk-modulation-and-demodulation-2/ [Accessed: 20 March 2020].

[87] S. N. Abdel-Razeq, A. S. Al-Azzeh, R.Y. Ayyoub, Study of QPSK Modulator and Demodulator in Wireless Communication System using MATLAB, *iJIM*, vol. 7, issue 2, pp. 4-8, April 2013.

[88] G. Breed, *Bit Error Rate: Fundamental Concepts and Measurement Issues, High Frequency Electronics*, pp. 46, 2003.

APPENDICES

VHF OSTBC MIMO Matlab Script

```
% Design antenna element and exciter
% Tilt antenna element to radiate in XY-plane, with boresight
along X-axis
fq = 135e6, 100e6, 70e6, ; % 135 MHz, 100 MHz, 70 MHz
y = design(yagiUda,fq);
y.Tilt = 90;
y.TiltAxis = 'Y';

% Create 4-by-4 antenna array
nrow = 4;
ncol = 4;
myarray = phased.URA('Size',[nrow ncol],'Element',y);

% Define element spacing to be half-wavelength at 135 MHz, 100
MHz and 70 MHz, and specify
% array plane as YZ-plane, which directs radiation in X-axis
direction
lambda = physconst('lightspeed')/fq;
drow = lambda/2;
dcol = lambda/2;
myarray.ElementSpacing = [drow dcol];
myarray.ArrayNormal = 'x';

% Display radiation pattern
figure
az = -180:1:180;
el = -90:1:90;
pattern(myarray,fq,az,el)
% tx parameters
tx = txsite('Name','Doringwater SS',...
    'Latitude',-29.08333333,...
```

```
    'Longitude',17.94527778,...
    'Antenna',myarray,...
    'TransmitterFrequency',fq,...
    'AntennaHeight',60,...
    'TransmitterPower',10);

% Define names for receiver sites, Each receiver has a
sensitivity of -107 dBm.

names = ["REC 4638","REC 4017"];
lats = [-28.89944444,-28.90111111];
lons = [18.13583333,18.13694444];

rx = rxsite('Name', names,...
       'Latitude',lats,...
       'Longitude',lons,...
       'AntennaHeight',60,...
       'ReceiverSensitivity',-107);
show(rx)

% Define signal strength levels (dBm) and corresponding colors
verystrongSignal = -60;
strongSignal = -70;
midSignal = -80;
weakSignal = -90;
veryweakSignal = -100;
edgeSignal = -107;
sigstrengths   =   [verystrongSignal   strongSignal   midSignal
weakSignal veryweakSignal edgeSignal];
sigcolors = {'blue' 'cyan' 'green' 'magenta' 'yellow' 'red'};

% Display coverage map. Specify Resolution of 50 m to get
% increased level of detail.
coverage(tx, ...
    'SignalStrengths',sigstrengths, ...
```

```
    'Colors',sigcolors);

ss = sigstrength(rx,tx);

% Define angles over which to perform sweep
azsweep = -30:10:30;

% Set up tapering window and steering vector
N = nrow*ncol;
nbar = 5;
sll = -20;
sltaper = taylorwin(N,nbar,sll)';
steeringVector = phased.SteeringVector('SensorArray',myarray);

for az = azsweep
    % Calculate and assign taper from steering vector
    sv = steeringVector(fq,[az; 0]);
    myarray.Taper = sltaper.*sv';

    % Update coverage map. Use greater resolution value to
improve speed of update.
    coverage(tx, ...
        'SignalStrengths',sigstrengths, ...
        'Colors',sigcolors);
end
```